iScience

CellPress
OPEN ACCESS

Article

D2R signaling in striatal spiny neurons modulates L-DOPA induced dyskinesia

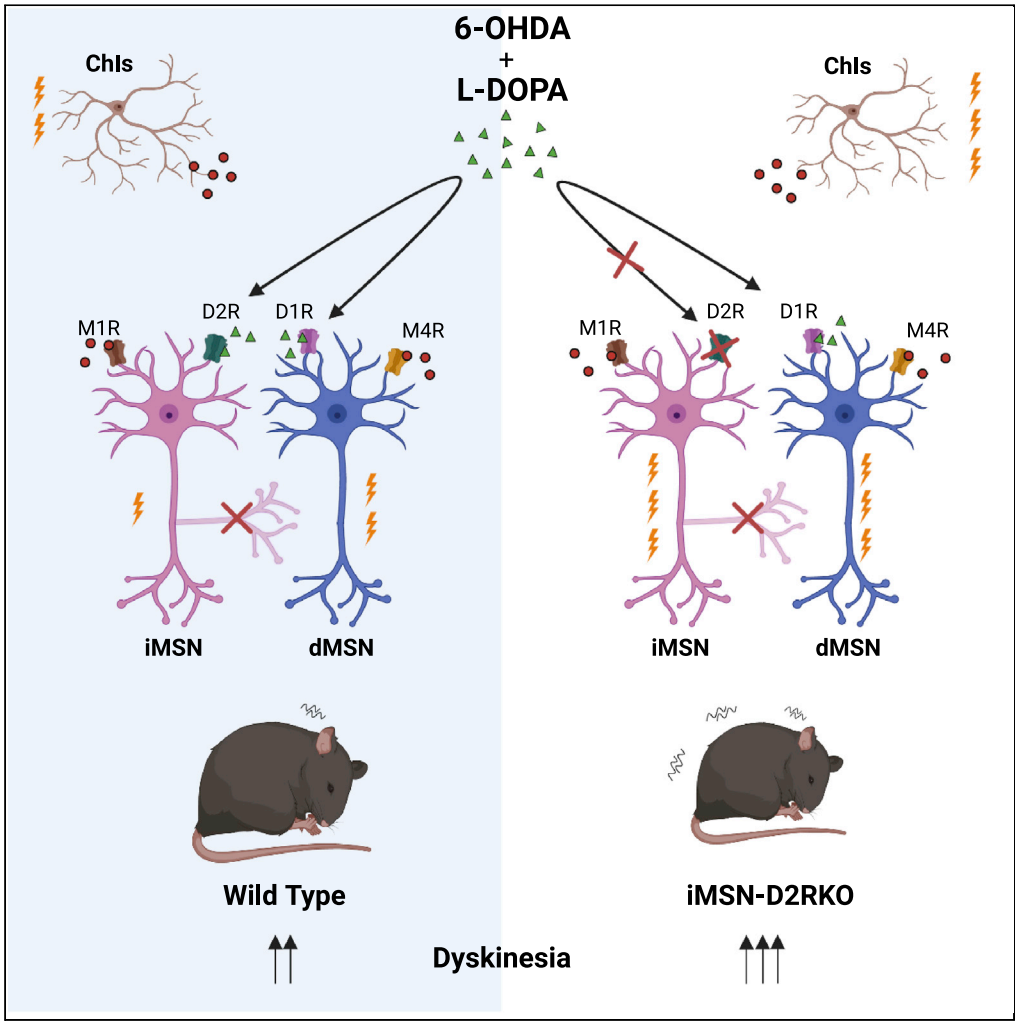

Ermanno Florio, Marcello Serra, Robert G. Lewis, ..., Marcello Wood, Micaela Morelli, Emiliana Borrelli

borrelli@uci.edu

Highlights

D2RKO in iMSNs increases L-DOPA-induced dyskinesia (LID)

D2R signaling in iMSNs inhibits striatal gene and PD-associated genes

Unopposed M1R signaling is responsible for the increased LID in iMSN-D2RKO mice

Simultaneous modulation of M1R and M4R signaling on MSNs drastically reduces LID

Florio et al., iScience 25, 105263
October 21, 2022
https://doi.org/10.1016/j.isci.2022.105263

iScience

CellPress
OPEN ACCESS

Article

D2R signaling in striatal spiny neurons modulates L-DOPA induced dyskinesia

Ermanno Florio,[1,5] Marcello Serra,[2,5] Robert G. Lewis,[1] Enikö Kramár,[3] Michael Freidberg,[4] Marcello Wood,[3] Micaela Morelli,[2] and Emiliana Borrelli[1,6,*]

SUMMARY

Degeneration of dopaminergic neurons leads to Parkinson's disease (PD), characterized by reduced levels of striatal dopamine (DA) and impaired voluntary movements. DA replacement is achieved by levodopa treatment which in long-term causes involuntary movements or dyskinesia. Dyskinesia is linked to the pulsatile activation of D1 receptors of the striatal medium spiny neurons (MSNs) forming the direct output pathway (dMSNs). The contribution of DA stimulation of D2R in MSNs of the indirect pathway (iMSNs) is less clear. Using the 6-hydroxydopamine model of PD, here we show that loss of DA-mediated inhibition of these neurons intensifies levodopa-induced dyskinesia (LID) leading to reprogramming of striatal gene expression. We propose that the motor impairments characteristic of PD and of its therapy are critically dependent on D2R-mediated iMSNs activity. D2R signaling not only filters inputs to the striatum but also indirectly regulates dMSNs mediated responses.

INTRODUCTION

Parkinson's disease (PD) is a severe neurological disorder characterized by impaired movements, dependent on the degeneration of DA neurons and the consequent reduction of DA-mediated control of striatal circuits. DA is a major modulator of striatal neuron activity, in particular of the medium spiny neurons (MSNs), expressing the two principal DA receptors, D1 and D2 (D1R, D2R). MSNs are also the only output neurons of the striatum. These neurons send feedback projections to the substantia nigra reticulata (SNr) and the internal portion of globus pallidus (GPi) either through the so-called direct MSNs (dMSNs), or through the indirect MSNs (iMSNs) (Alexander and Crutcher, 1990; Gerfen and Surmeier, 2011). Relevant to PD studies, while the genetic ablation of D1R in mice does not affect basal motor activity (Xu et al., 1994), loss of D2Rs either in constitutive or iMSNs-specific knockout mice results into slow movements and loss of coordination with great similarities with PD motor symptoms (Anzalone et al., 2012; Baik et al., 1995; Lemos et al., 2016).

These results agree with the conventional models of basal ganglia (Albin et al., 1989; Gerfen and Surmeier, 2011), whereas the activation of striatal D2R by decreasing iMSNs activity facilitates movement. D2R signaling on iMSNs also controls intrastriatal circuits through the regulation of GABA release from collaterals (Dobbs et al., 2016; Kharkwal et al., 2016; Lemos et al., 2016).

Administration of the DA precursor levodopa (L-DOPA) is commonly used to treat PD. However, the positive anti-akinetic effects of L-DOPA are counterbalanced by the development, upon long-term use, of dyskinesia, a debilitating motor condition characterized by the appearance of hyperkinetic and dystonic involuntary movements affecting the face, body extremities, and the trunk (Bastide et al., 2015); this pathology appears linked to the over-activation of D1R signaling in dMSNs (Fasano et al., 2010; Santini et al., 2012). Indeed, 6-hydroxydopamine (6-OHDA) D1R knockout (KO) mice treated with L-DOPA are not dyskinetic (Darmopil et al., 2009) indicating that the pulsatile activation of dMSNs is responsible for L-DOPA-induced dyskinesia (LID). Whether and how activation of D2Rs in iMSNs has a role in LID is less clear.

The heterogeneous expression of D2Rs in several striatal neurons and afferences has prevented the cell-specific analysis of the implication of D2R signaling in LID. Indeed, D2Rs in addition to iMSNs are also expressed by cholinergic interneurons (ChIs); and acetylcholine (ACh) signaling appears also to be involved in LID (Ding et al., 2011; Won et al., 2014) as the administration of L-DOPA increases ChIs excitability, while ChIs ablation alleviates LID (Ding et al., 2011; Won et al., 2014) in the 6-OHDA model of PD.

[1]Department of Microbiology & Molecular Genetics, INSERM U1233, Center for Epigenetics and Metabolism, 308 Sprague Hall, University of California, Irvine, Irvine, CA 92697, USA

[2]Department of Biomedical Sciences, Section of Neuroscience, University of Cagliari, Cittadella Universitaria di Monserrato, 09042 Monserrato (CA), Italy

[3]Department of Neurobiology and Behavior, University of California, Irvine, 200 Qureshey Research Lab., Irvine, CA 92697, USA

[4]Department of Chemistry, University of California, Irvine, 1102 Natural Sciences II, Irvine, CA 92697, USA

[5]These authors contributed equally

[6]Lead contact

*Correspondence: borrelli@uci.edu

https://doi.org/10.1016/j.isci.2022.105263

Thus, to address the involvement of D2R in LID, we performed hemilateral lesion of dopaminergic neurons in iMSN-D2RKO and WT littermates using 6-OHDA followed by repeated treatments with L-DOPA to induce the expression of abnormal involuntary movements (AIMs), the equivalent of LID in humans. Turning behavior upon lesion was assessed in mice of both genotypes, and dyskinesia-like AIMs were quantified following L-DOPA administration. Brains of mice were analyzed at multiple levels. Importantly, analyses of the dorsolateral striatum (DLS) of mice of both genotypes showed an exaggerated response of iMSN-D2RKO mice reflected on all parameters tested, in particular in AIMs intensity and associated markers. The behavioral and cellular phenotypes were accompanied by reprogramming of transcriptomics in the DLS and affect genes previously involved in PD. Interestingly, the increased AIMs of iMSN-D2RKO mice could be brought back to WT levels by selectively blocking the muscarinic receptor type 1 (M1R). In addition, when the M1R antagonist was used in combination with a positive allosteric modulator of muscarinic receptor type 4 (M4R), L-DOPA-induced AIMs were drastically reduced in both genotypes. These results show the importance of DA-mediated control on ACh and its involvement in AIMs. Altogether our results indicate that D2R signaling in iMSNs is highly involved in the motor deficits of PD and LID by inhibiting and counterbalancing the cholinergic stimulation of iMSNs and dMSNs.

RESULTS

Dopamine receptors type 2 signaling in iMSNs is critically involved in the regulation of motor functions

iMSN-D2RKO mice have been genetically modified to selectively remove D2Rs from iMSNs (Figure 1A; Anzalone et al., 2012; Kharkwal et al., 2016). To analyze the consequences of dopamine depletion induced by the 6-OHDA lesion of DA neurons on motor activity and more importantly on the expression of AIMs, iMSN-D2RKO and WT siblings received a unilateral stereotaxic injection in the DLS of either saline or 6-OHDA, a retrogradely transported toxin that kills dopaminergic neurons (Lundblad et al., 2005). We achieved more than 90% depletion of dopaminergic neurons from the substantia nigra compacta (SNc), as shown by immunofluorescence analyses using tyrosine hydroxylase (TH), a marker of DA neurons (Figures 1B and S1A). Interestingly, we observed a higher mortality rate in WT as compared to iMSN-D2RKO mice in response to 6-OHDA (21.82% for WT (n = 52) versus 9.59% for iMSN-D2RKO (n = 48); Figure S1B). Three weeks after surgery, sham and 6-OHDA mice were tested in the open field to quantify their forward motor activity (Figure 1C), as well as the total number of ipsi/contralateral rotations (used as index of asymmetry) over a period of 10 min (Figures 1D and 1E). As expected, hemi-parkinsonian WT mice showed a dramatic reduction in the total distance traveled ($p < 0.0001$; Figure 1C), and a significant increase in the asymmetry index (ratio of ipsilateral/total rotation), when compared to sham mice of the same genotype ($p < 0.0001$; Figure 1D). In iMSN-D2RKO mice, 6-OHDA lesions produced minor additional motor deficits (forward locomotion: mean diff. sham vs 6-OHDA, WT: 3601, iMSN-D2RKO: 1837; $p < 0.0001$; Figure S1C), and a significant increase of the asymmetry index ($p < 0.0001$; Figure 1D). Of note, we found that 6-OHDA iMSN-D2RKO mice performed significantly less ipsilateral rotations ($p < 0.001$; Figure 1E) as compared to WT mice. Additionally, the number of ipsilateral rotations between sham and 6-OHDA iMSN-D2RKO mice, which is determined by the unbalance stimulation of striatal D1/D2R following 6-OHDA infusion in only one hemisphere (Wang and Zhou, 2017), was not statistically significant between iMSN-D2RKO sham and lesioned mice ($p > 0.05$; Figure 1E), although TH staining confirmed DA neurons loss in iMSN-D2RKO mice (Figure S1A). These results well illustrate how the absence of D2R signaling in both hemispheres affects the lateralized sensorymotor integration and forelimb akinesia induced by the 6-OHDA lesion.

Gene expression profiles of the dorsolateral striatum of 6-hydroxydopamine-lesioned iMSN-D2RKO and wild-type mice

Mice of both genotypes were sacrificed, and brains were flash frozen. Punches of the DLS were obtained on cryostat sections and processed for RNA extraction to prepare the library. RNA-seq analyses were then made to obtain molecular footprints of the DLS of mice of both genotypes. Three weeks after surgeries, both WT and iMSN-D2RKO mice were treated daily for 11 days with either saline (group 1 and 2) or L-DOPA (group 3) at 15 mg/kg (s.c.). Three experimental groups were thus used and analyzed: 1) sham-lesioned (sham); 2) 6-OHDA-lesioned (6-OHDA); and 3) 6-OHDA lesioned/L-DOPA-treated (L-DOPA). Differentially expressed genes (DEGs) between treatments in the same genotype and between genotypes are shown in Table S1.

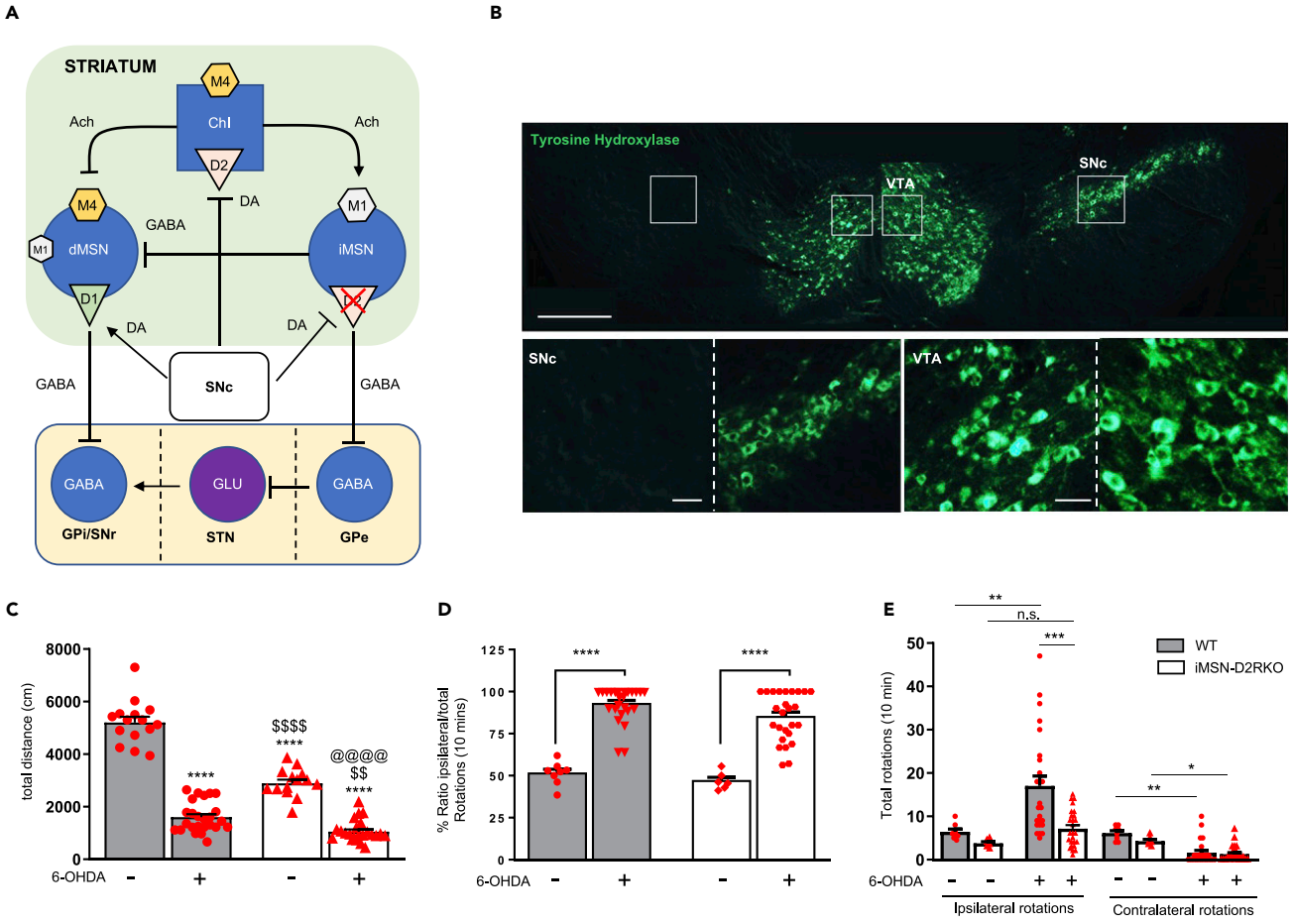

Figure 1. Characterization of unilateral 6-hydroxydopamine (6-OHDA) lesions in WT and iMSN-D2RKO mice

(A) Schematic depicting the direct and indirect striatal pathways in iMSN-D2RKO mice. Lines with arrowheads indicate neuronal activation, while blunt-ended lines indicate neuronal inhibition, the loss of D2R expression is indicated by a red cross. Abbreviations: ACh, acetylcholine; ChI, cholinergic interneurons; GABA, γ-aminobutyric acid; GPi/GPe, internal/external portion of globus pallidus; DA, dopamine; SNc, substantia nigra compacta; SNr, substantia nigra reticulata; STN, subthalamic nucleus.

(B) Representative immunofluorescent images of tyrosine hydroxylase (TH) on a coronal section including the SNc and ventral tegmental area (VTA). Note the absence of staining of the SNc on the left side after striatal 6-OHDA infusion while the VTA appears unaffected. Scale bars: 500 μm (upper panel); 50 μm (lower panels).

(C) Motor activity in the open field (10 min) by sham (–) and 6-OHDA (+) WT (grey) and iMSN-D2RKO (white) mice (N = 14-15 for sham; 23-25 for 6-OHDA-lesioned). ****p < 0.0001 vs sham WT; $$ p < 0.01, $$$$ p < 0.0001 vs 6-OHDA WT; @@@@ p < 0.0001 vs sham iMSN-D2RKO; 2way ANOVA followed by Bonferroni post-hoc analysis. Significant interactions were observed for genotype p < 0.0001 ($F(1, 73) = 109$), lesion p < 0.0001 ($F(1, 73) = 391.2$), and genotype × lesion p < 0.0001 ($F(1, 73) = 41.13$).

(D) Percentage values showing the ratio of ipsilateral/total body rotations performed in 10 min by sham (–) and 6-OHDA (+) WT (gray) and iMSN-D2RKO mice (white) (N = 6-8 for sham; 23-25 for 6-OHDA-lesioned). ****p < 0.0001 vs sham of the same genotype. 2way ANOVA followed by Bonferroni post-hoc analysis showed a significant percentage of increase of the ratio in lesioned mice p < 0.0001 ($F(1, 61) = 125.7$).

(E) Bar graph indicating the total number of ipsilateral (left), and contralateral (right) rotations performed during 10 min by sham (–) and 6-OHDA (+) WT and iMSN-D2RKO mice. *p < 0.05, **p < 0.01, ***p < 0.001. 2way ANOVA followed by Bonferroni post-hoc analysis, Ipsilateral: lesion p < 0.0001 ($F(1, 61) = 8.426$), and genotype p = 0.021 ($F(1, 61) = 6.097$; contralateral: lesion p < 0.005 ($F(1, 61) = 32.61$), and genotype p = 0.016 ($F(1, 61) = 5.546$). All data are expressed as mean values ± SEM. See also Figure S1.

Absence of dopamine receptors type 2 signaling in iMSNs leads to the reprogramming of striatal gene expression

DEGs in the DLS of the sham groups of WT and iMSN-D2RKO striata were identified using a threshold of at least 20% of fold change and an adjusted p value of <0.1. These analyses identified 251 DEGs in iMSN-D2RKO versus WT DLS (Figure 2A and Table S1); of these, only a small proportion (37) were down-regulated while the vast majority (214) were up-regulated (Figure 2B). The observed up-regulation of genes in the DLS

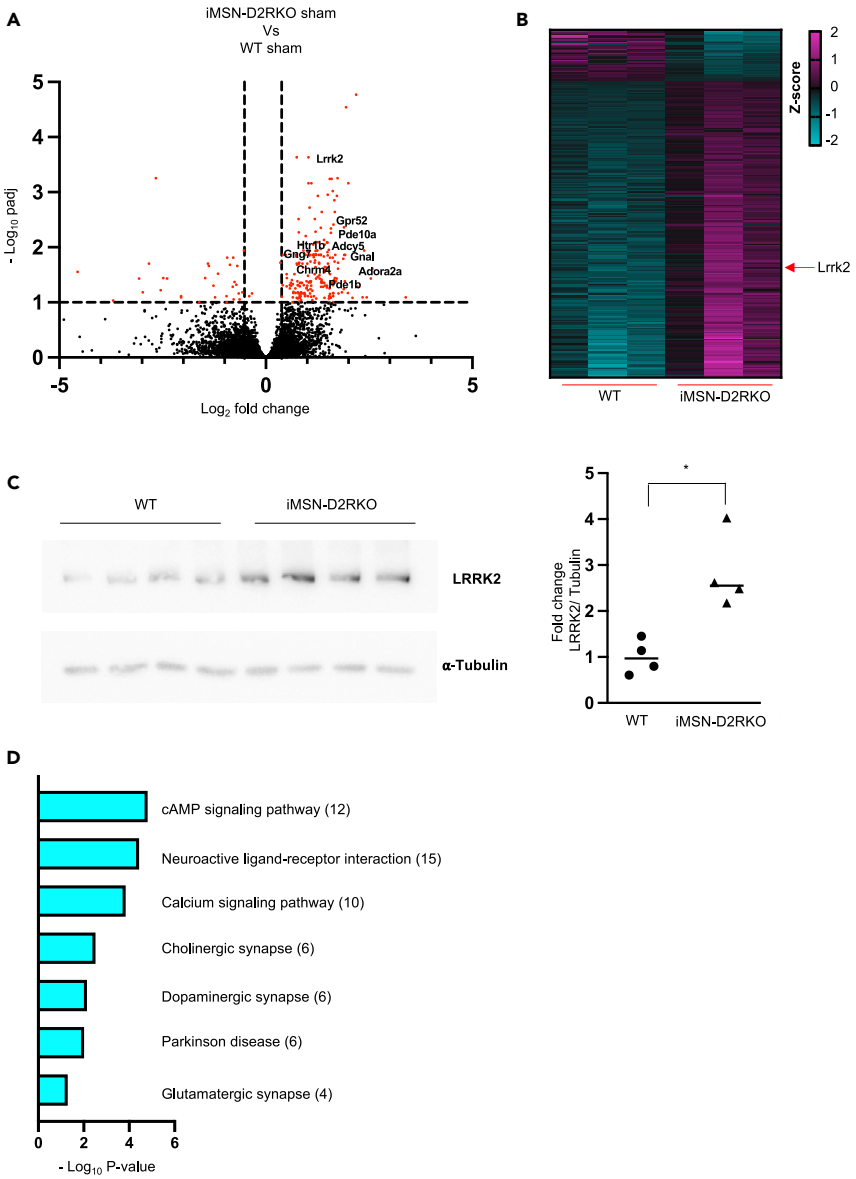

Figure 2. Differential gene expression in the DLS between WT and iMSN-D2RKO sham

(A) Volcano plot based on the −log10 adjusted p value versus the $\log_2$ Fold Change (FC) of the DLS transcriptome. Cut-offs are shown as dotted lines (p-adj < 0.01) and log2FC ± 20%.

(B) Heat-map representing the single mouse z-score (distance of each raw score from the mean) of the 251 statistically significant DEG (p-adj < 0.1).

(C) Representative Western blot analyses of LRRK2 from WT and iMSN-D2RKO sham DLS protein extracts. Protein concentration was normalized on α-tubulin. Quantifications are shown in the graph as fold change with the WT arbitrarily set to 1. t-test significant for *p < 0.01.

(D) KEGG pathway analysis of enriched pathways containing the 252 DEGs between WT and iMSN-D2RKO sham mice. KEGG p-value <0.05 (-Log10), the numbers in brackets represent the number of genes in each pathway. See also Table S1.

of iMSN-D2RKO likely reflects, at the gene expression level, the lack of the inhibitory control exerted by D2R signaling in the iMSNs on striatal circuits. Strikingly, among up-regulated genes, the Leucine-Rich Repeat Kinase 2 (LRRK2) stood out, whose dysfunctional expression and/or mutations have been linked to PD (Figures 2A and 2B) (Mandemakers et al., 2012; Tozzi et al., 2018). We confirmed that the LRRK2 RNA up-regulation in iMSN-D2RKO was also reflected at the protein level, as illustrated by Western blot analyses of DLS extracts (p < 0.01; Figure 2C).

Next, we aimed at identifying the pathways containing the DEGs, using the KEGG analysis performed with "ENRICHR" tool ($p < 0.05$) (Chen et al., 2013). These analyses highlighted identified signal transduction pathways known to regulate striatal functions (Figure 2D). Among them, the cAMP pathway emerged which included the Adenylate Cyclase 5 (ADCY5) (Lee et al., 2002), the α-subunit of G-olf (GNAL) (Jiang et al., 2001), the γ-subunit 7 (GNG7) of the heterotrimeric G-proteins (Schwindinger et al., 2010) as well as the phosphodiesterases PDE10A, PDE7B, PDE1B which regulate cAMP and cGMP levels (Table S1) (de Gortari and Mengod, 2010; Gresack et al., 2014). We also identified membrane receptors involved in the regulation of motor functions, positively coupled to the cAMP pathway, and specifically expressed in iMSNs, such as ADORA2A and GPR52, as well as, the muscarinic receptor type 4, which is highly expressed in dMSNs (Komatsu et al., 2014; Shen et al., 2015; Siokas et al., 2021), and the serotonin receptors HTR2A and HTR1B previously linked to PD and LID (Lee et al., 2012).

More importantly, most of the DEGs were previously identified upon 6-OHDA lesions in WT animals (Morales-Garcia et al., 2011; Park et al., 2014). Thus, loss of D2R signaling in iMSNs generates a reprogramming of gene expression with similarities to changes in gene expression in the DA-deprived striatum.

6-hydroxydopamine ablation of dopamine neurons differentially affects gene expression in the dorsolateral striatum of wild type and dopamine receptors type 2 mutants

Next, we performed comparisons of RNA-seq results between 6-OHDA and sham-lesioned mice of the same genotype. Dopamine deprivation induced gene expression changes in both genotypes, as expected. However, the DEGs in the WT were ~half (717; padj<0.1), of that in the iMSN-D2RKO (1532; padj<0.1) (Figures 3A and 3B, and Table S1). Venn diagrams analyses of the DEGs showed that 236 were in common between 6-OHDA WT and iMSN-D2RKO DLS (Figure 3B); of these the large majority were down-regulated in both genotypes upon dopamine depletion (Figure 3C). KEGG analyses of these genes showed their involvement in critical striatal signaling (Figure 3D).

Gene Ontology (GO) analyses (Figure S2A) of molecular functions of DEGs specific to the 6-OHDA WT DLS, showed an abundance of genes belonging to GABA signaling. On the contrary, in the iMSN-D2RKO, DEGs belonged to glutamatergic signaling pathways (Figure S2B).

Importantly, in the iMSN-D2RKO DLS following the 6-OHDA lesion, the 78 genes up-regulated in sham conditions were no longer found, indicating the involvement of dopamine in the activation of their expression (Figure S3A). These genes were also down-regulated in the WT, further supporting the role of DA in their expression (Figure S3B). Importantly, in this group, we identified genes differentially expressed in iMSN-D2RKO sham versus WT and associated with PD, such as ADCY5, LRRK2, CHRM4, AKAP5, GPR52, RYR3, PDE10a, RGS4, and GPR88 (Morales-Garcia et al., 2011; Nicolini et al., 2015; Park et al., 2014; Wennogle et al., 2017). Thus, the removal of D2R signaling from iMSNs generates the up-regulation of critical genes in sham conditions, which is then counteracted by loss of DA, suggesting that these genes are dependent upon D1R signaling.

We also identified twenty-four genes whose expression changed in WT mice following 6-OHDA lesion, but not in iMSN-D2RKO DLS (Figure S3C), suggesting a D2R-mediated control of their expression in iMSNs. One such gene is GPR6, which is indeed principally expressed in iMSNs (Ho et al., 2018) and whose function has been previously associated with dyskinesia in rodent models of PD (Oeckl et al., 2014).

Our analyses identified 76 genes differentially expressed only in iMSN-D2RKO after the 6-OHDA lesion. Their differential expression in the iMSN-D2RKO suggests that they might be either directly regulated by D2R signaling in iMSNs, or indirectly in dMSNs, such as GNAL (Figure S3D) (Goto, 2017).

Loss of dopamine receptors type 2 in iMSNs further exacerbates L-DOPA-induced dyskinesia and impairs striatal synaptic plasticity

To determine the consequences of D2R loss in iMSNs over L-DOPA-induced dyskinesia, 6-OHDA WT and iMSN-D2RKO mice were treated for 11 consecutive days with L-DOPA (15 mg/kg, s.c.) plus benserazide (12 mg/kg, s.c.). This dosage regimen is effective in the promotion and maintenance of dyskinetic AIMs, affecting axial, limb, and orolingual (ALO) muscles (Bido et al., 2011; Santini et al., 2007). Cumulative ALO AIMs, scored at 1, 4, 7, and 10 days of L-DOPA treatment revealed that iMSN-D2RKO mice expressed

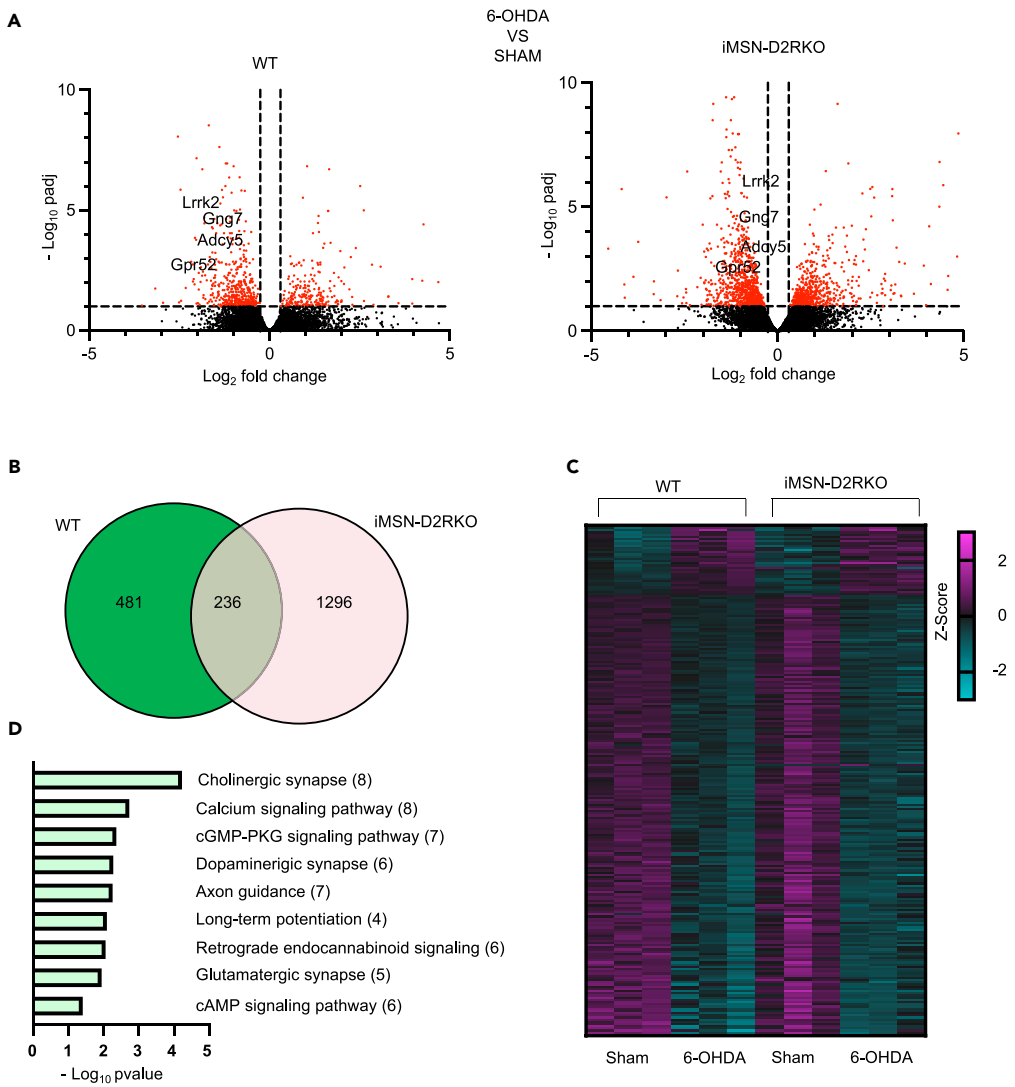

Figure 3. Differential gene expression upon 6-OHDA lesion in WT and iMSN-D2RKO DLS

(A) Volcano plot based on the −log10 adjusted p value versus the log2FC of the DLS transcriptome (6-OHDA vs sham mice in both genotype). Cut-offs are shown as dotted lines (p-adj < 0.01) and log2FC ± 20%.

(B) Venn-diagram representing the common and the exclusive genes of the two differential expression analyses (6-OHDA WT vs sham WT and 6-OHDA iMSN-D2RKO vs sham iMSN-D2RKO mice).

(C) Heatmap representing the single mouse z-score of the 236 statistically significant common genes shown in B, adjusted p value > 0.1.

(D) KEGG pathway analysis of the 236 statistically significant common genes shown in B. All pathways are significant for p value <0.05 (shown as -Log10), the numbers in brackets represent the number of genes for each pathway. See also Figures S2 and S3 and Table S1.

significantly higher cumulative AIMs, when compared to WT mice ($p < 0.05$, Figure 4A). The increased AIMs in L-DOPA iMSN-D2RKO mice were observed in all types of dyskinetic movements (Figure S4).

Interestingly, the higher sensitivity to LID of iMSN-D2RKO mice was linked to the treatment length (Figure 4B). Bonferroni post-hoc test of 2-way ANOVA repeated measures (RM) analyses revealed that L-DOPA iMSN-D2RKO mice manifest a significant worsening of LID starting at day 4 of treatment ($p < 0.05$; Figure 4B), reaching the peak at day 10 ($p < 0.01$; Figure 4B) as compared to time-matched L-DOPA WT mice. Time course analyses also revealed that the widest difference between L-DOPA iMSN-D2RKO and WT mice takes place on day 10, during the first 40 min that follow administration,

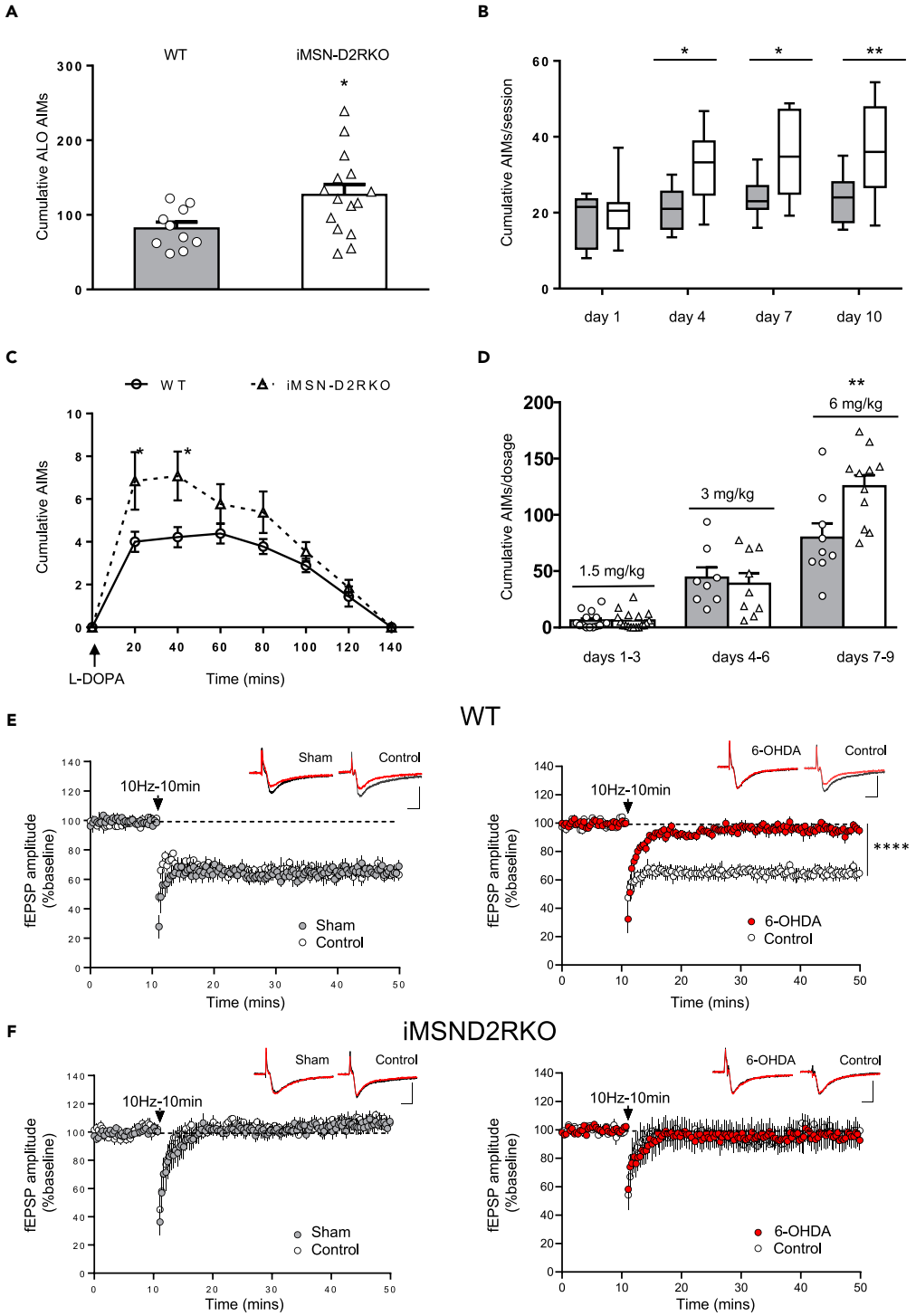

Figure 4. Removal of D2R in iMSN exacerbates L-DOPA-induced abnormal involuntary movements (AIMs) and impairs striatal LFS-LTD

(A) Bar graph showing the cumulative axial-limb-orolingual (ALO) abnormal involuntary movements (AIMs) scores measured on day 1, 4, 7, and 10 of chronic L-DOPA (N = 10-15/group). *p < 0.05 vs WT. Mann Whitney non-parametric two-sided t-test (p = 0.0254).

(B) Box plot showing the ALO AIMs scores measured at day 1, 4, 7, and 10 of L-DOPA treatment (N = 10-15/group). Boxplots indicate the top and bottom quartiles; whiskers refer to top and bottom 90%. *p < 0.05, **p < 0.01 vs WT. 2way

Figure 4. *Continued*

ANOVA repeated measures (RM) followed by Bonferroni post-hoc analysis. The 2way ANOVA RM is significant × genotype $p = 0.0030$ ($F (1, 23) = 11.55$), and × time $p < 0.0001$ ($F (2.68, 50.99) = 10.18$).

(C) Time course showing the ALO AIMs expression after L-DOPA treatment (day 10) (N = 10-15/group). *$p < 0.05$ vs WT. 2way ANOVA RM followed by Bonferroni post-hoc analysis. The 2way ANOVA RM is significant × genotype $p = 0.0482$ ($F (1, 20) = 4.426$), × time $p < 0.0001$ ($F (2.33, 46.63) = 18.52$), and genotype × time $p = 0.0175$ ($F (5, 100) = 2.894$).

(D) Bar graph showing the cumulative ALO AIMs scores measured after ascending doses of L-DOPA:1.5 mg/kg (days 1-3), 3 mg/kg (days 4-6), and 6 mg/kg (days 7-9). Results were obtained in medial forebrain bundle (MFB) 6-OHDA-lesioned WT and iMSN-D2RKO mice (N = 9-15/group). 2way ANOVA followed by Bonferroni post-hoc analysis. The 2way ANOVA is significant × genotype $p = 0.0398$ ($F (1, 59) = 4.418$), × L-DOPA dose $p < 0.0001$ ($F (2, 59) = 92.95$), and genotype × L-DOPA dose $p = 0.0025$ ($F (2, 59) = 6.646$). Data are expressed as mean values, error bars represent SEM.

(E) Graphs showing striatal field potential recordings from control, sham (left), and 6-OHDA WT (right) mice before (basal) and following the delivery of low-frequency stimulations (LFS). LFS induced a robust striatal long-term depression (LTD) in control (N = 3, left; N = 6, right) and sham WT mice (N = 6), while failed to induce striatal LTD in 6-OHDA WT mice (N = 6). fEPSP is normalized to baseline, averaged (mean ± SEM), and plotted as a function of time. ****$p < 0.0001$ vs 6-OHDA WT. 2way ANOVA RM followed by Bonferroni post-hoc analysis. The 2way ANOVA RM is significant × time $p < 0.0001$ ($F (155, 1550) = 26.28$), × lesion $p < 0.0001$ ($F (1, 10) = 37.44$), and time × lesion $p < 0.0001$ ($F (155, 1550) = 11.87$). Bar scale; 0.2 mV/5ms.

(F) Graphs showing striatal field potential recordings from control, sham (left), and 6-OHDA iMSN-D2RKO (right) mice before (basal) and following the delivery of LFS. LFS failed to induce striatal LTD in control (N = 6), sham (N = 7), and 6-OHDA iMSN-D2RKO mice (N = 6). fEPSP is normalized to baseline, averaged (mean ± SEM), and plotted as a function of time. Bar scale; 0.2 mV/5ms. Inset: representative baseline traces in black and 40 min post-LFS in red. Bar scale; 0.4 mV/5ms. See also Figure S4.

when DA concentration is reportedly higher (Lindgren et al., 2010; Meissner et al., 2006) ($p < 0.05$; Figure 4C). These results indicate that loss of the dopaminergic control of iMSNs sensitizes the striatal circuit and increases LID expression, and strongly highlights the critical role of D2R signaling in these neurons as a required filter in the regulation of striatal motor responses.

As LID is affected both by the extent of nigrostriatal neurons' degeneration and by the dose of L-DOPA (Bastide et al., 2015; Deurwaerdère et al., 2017), we also evaluated the same parameters using mice of both genotypes receiving ascending doses of L-DOPA (1.5, 3, 6 mg/kg, s.c.) plus benserazide (12 mg/kg, s.c), three weeks after the stereotaxic injection of 6-OHDA in the medial forebrain bundle (MFB) (Cenci and Crossman, 2018). Similar to results obtained after striatal lesions, AIMs analyses of MFB 6-OHDA-lesioned (MFB 6-OHDA) mice revealed a dose-dependent effect of L-DOPA in both genotypes (Figure 4D). MFB 6-OHDA iMSN-D2RKO mice showed a higher dose-dependent susceptibility towards the pro-dyskinetic effects of L-DOPA as compared to similarly treated WT mice. Interestingly, while no differences were observed between genotypes at 1.5 and 3 mg/kg of L-DOPA, the administration of 6 mg/kg of L-DOPA in MFB 6-OHDA iMSN-D2RKO mice, significantly increased the expression of AIMs when compared to WT controls ($p < 0.01$; Figure 4D). These results suggest a D2R-dependent mechanism that counters above-threshold/excessive DA signaling in the striatum.

Striatal D2R signaling plays a critical role in the generation of long-term depression (LTD) at corticostriatal synapses (Calabresi et al., 1997; Kreitzer and Malenka, 2005). Abnormal striatal plasticity is considered a key factor involved in the development of PD symptoms as well as LID (Picconi et al., 2003; Shen et al., 2008; Thiele et al., 2014). Thus, we evaluated long-term depression by measuring the excitatory postsynaptic field potentials (fEPSP) in DLS coronal slices of the DLS of control (no surgery), sham, and 6-OHDA WT and iMSN-D2RKO mice. fEPSP were registered before and after the delivery of a 10 min continuous train of low-frequency stimulation (LFS) in the DLS. Delivery of LFS in coronal striatal slices produces a robust and long-lasting LTD in both control and sham WT slices (Figure 4E, left; WT: control, 64% ± 4%, $p < 0.001$; sham, 65% ± 5%, $p < 0.001$) which did not differ in magnitude or kinetics (Figure 4E, left; rmANOVA: surgery × time interaction, $F_{155,\ 1085} = 0{,}965$, $p = 0.602$) (Kreitzer and Malenka, 2005; Ronesi and Lovinger, 2005). On the contrary, LFS delivery in control and sham iMSN-D2RKO slices did not change fEPSP amplitude (Figure 4F, left; iMSN-D2RKO: control, 102% ± 4%, $p > 0.05$; sham, 103% ± 3%, $p > 0.05$; rmANOVA: surgery × time interaction, $F_{155,\ 1705} = 0.521$, $p > 0.999$). Loss of DA signaling prevented the generation of LFS-LTD in the striatum of 6-OHDA WT mice (Figure 4E, right; WT: control, 65% ± 3.7%, $p < 0.05$, 6-OHDA, 96% ± 2.9%, $p > 0.05$; rmANOVA: surgery × time interaction, $F_{155,\ 1550} = 11.87$, $p < 0.0001$) (Kreitzer and Malenka, 2007; Lerner and Kreitzer, 2012). Interestingly, in iMSN-D2RKO slices, LTD was not observed whether we tested the control or the 6-OHDA hemispheres (Figure 4F, right;

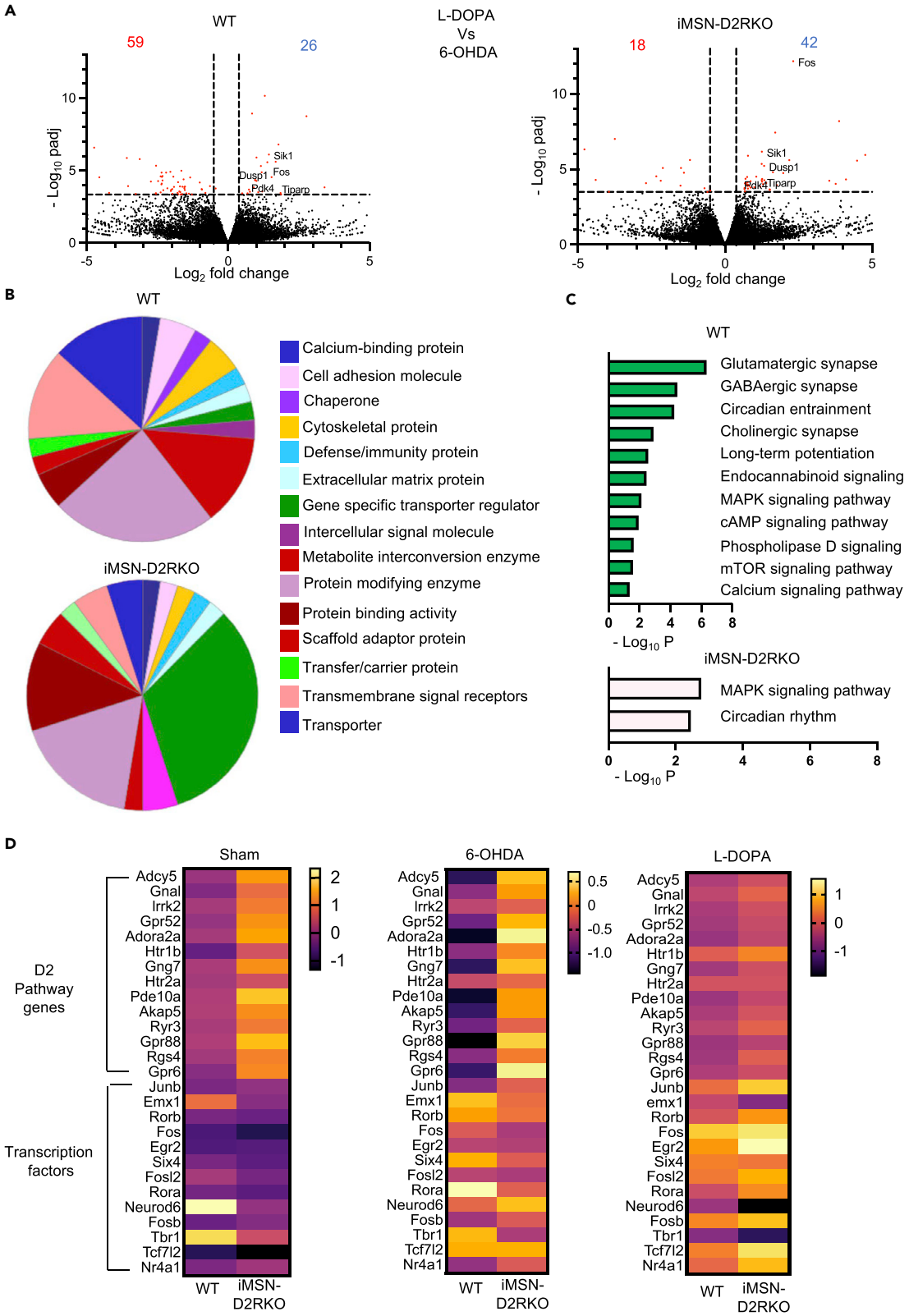
A
WT
59
26
L-DOPA
Vs
6-OHDA
iMSN-D2RKO
18
42
Fos
Sik1
Dusp1
Pdk4
Tiparp
- Log10 padj
Log2 fold change
B
WT
iMSN-D2RKO
Calcium-binding protein
Cell adhesion molecule
Chaperone
Cytoskeletal protein
Defense/immunity protein
Extracellular matrix protein
Gene specific transporter regulator
Intercellular signal molecule
Metabolite interconversion enzyme
Protein modifying enzyme
Protein binding activity
Scaffold adaptor protein
Transfer/carrier protein
Transmembrane signal receptors
Transporter
C
WT
Glutamatergic synapse
GABAergic synapse
Circadian entrainment
Cholinergic synapse
Long-term potentiation
Endocannabinoid signaling
MAPK signaling pathway
cAMP signaling pathway
Phospholipase D signaling
mTOR signaling pathway
Calcium signaling pathway
- Log10 P
iMSN-D2RKO
MAPK signaling pathway
Circadian rhythm
- Log10 P
D
Sham
6-OHDA
L-DOPA
D2
Pathway
genes
Transcription
factors
Adcy5
Gnal
Irrk2
Gpr52
Adora2a
Htr1b
Gng7
Htr2a
Pde10a
Akap5
Ryr3
Gpr88
Rgs4
Gpr6
Junb
Emx1
Rorb
Fos
Egr2
Six4
Fosl2
Rora
Neurod6
Fosb
Tbr1
Tcf7l2
Nr4a1
WT
iMSN-D2RKO

Figure 5. Differential gene expression between L-DOPA WT vs 6-OHDA WT and L-DOPA iMSN-D2RKO vs 6-OHDA iMSN-D2RKO mice

(A) Volcano plot based on the −log10 adjusted p value versus the log2FC of the DLS transcriptome (L-DOPA mice vs 6-OHDA mice in both genotypes). Cut-offs are shown as dotted lines (p-adj < 0.01) and log2FC ± 20%. The numbers in red refer to downregulated genes, the numbers in blue refer to up-regulated genes with respect to the 6-OHDA mice. The genes named in the volcano plot are the 5 common genes observed in 6-OHDA WT and iMSN-D2RKO mice following L-DOPA treatment. (B) Pie charts represent protein functionality analysis of DEGs for WT and iMSN-D2RKO mice after L-DOPA treatment. The most representative categories are shown in the legend.

(C) KEGG pathway analysis showing the most enriched pathways respectively to the comparison of L-DOPA vs 6-OHDA mice of each genotype. KEGG p-value <0.05 (shown as -Log10).

(D) Three heat maps (sham, 6-OHDA, L-DOPA) representing differences in expression (z-score) between WT and iMSN-D2RKO mice of genes related to D2 pathway activation and several transcription factors.

iMSN-D2RKO: control, 93% ± 1.9%, $p > 0.05$; 6-OHDA 95% ± 8.9%, $p > 0.05$; rmANOVA: surgery × time interaction, $F_{155,\ 1395} = 0.392$, $p > 0.999$).

Overall, these results extend previous knowledge obtained using constitutive D2R knockout mice, demonstrating that the LTD that follows the stimulation of corticostriatal fibers (Calabresi et al., 1997) depends on the cell-specific activation of D2R in iMSNs.

L-DOPA treatment partially restores the dorsolateral striatum transcription profiles in wild type, but not in iMSN-D2RKO

The increased AIMs that follow L-DOPA treatment in iMSN-D2RKO brought us to analyze the presence of changes at the gene expression level in the DLS of these mice as compared to WT. Comparisons of DEGs (padj<0.1; Table S1 and Figure 5A), before and after chronic L-DOPA treatments of 6-OHDA lesioned mice showed the presence of only five coding genes in common between the two genotypes: c-fos, Sik1, Dusp1, Tiparp, and Pdk4 (Figure 5A). Importantly, despite the presence of c-fos in both genotypes, a much larger increase of its expression was found in iMSN-D2RKO as compared to WT (after L-DOPA, iMSN-D2RKO: 2.32 fold (p=1.25E-08) and WT:1.67 fold (p = 0.0035) above saline treated). Notably, after L-DOPA, the majority of DEGs were downregulated in the WT, while in the iMSN-D2RKO were upregulated (Figure 5A). Similar ratios between up- and down-regulated genes were also obtained with the adjusted p-value raised to 0.2 or 0.3. In the iMSN-D2RKO DEGs, our analyses identified as the target of the differential expression some genes previously linked to LID, such as Nr4a1 (Rouillard et al., 2018), GPR3 (Patricio et al., 2020) and SNCA (Martikainen et al., 2015).

In the WT, KEGG ($p < 0.05$) and protein function analyses highlighted pathways involved in synapse formation and functions (Figures 5B and 5C). This was not the case in iMSN-D2RKO, where the majority of DEGs were associated with pathways connected to the control of transcription (Figures 5B and 5C).

We also retrieved and compared, between genotypes and conditions, MSN-specific differentially expressed genes (Figure 5D). Interestingly, in all conditions, iMSN-D2RKO DLS showed the most accentuated expression changes, as compared to WT mice (Figure 5D). These results support the view of D2R-dependent signaling in iMSNs being required for the general control of striatal gene expression.

Dopamine receptors type 2 on iMSNs modulate direct output pathway activity

LID has been correlated with the pathological activation of hypersensitive D1Rs in dMSNs, and the consequent potent activation of the direct pathway (Santini et al., 2012). At the cellular level, LID is mirrored by the increased phosphorylation of the extracellular signal-regulated kinase ($pERK^{42/44}$) and of the downstream target c-Fos (Santini et al., 2007; Valjent et al., 2000; Westin et al., 2007). L-DOPA administration greatly increased $pERK^{42/44}$ and c-Fos immunoreactivity in the DLS of 6-OHDA mice of both genotypes as compared to equally treated sham ($p < 0.0001$; Figures 6A and 6B) (Cortés et al., 2017; Santini et al., 2007). Notably, following acute L-DOPA, 6-OHDA iMSN-D2RKO mice showed a trend toward increased of $c\text{-}Fos^{+}$ cells and of $pERK^{42/44}$ intensity/cell as compared to equally treated 6-OHDA WT ($p > 0.05$; Figures S5A–S5C). However, following chronic L-DOPA, a statistically significant increase of $pERK^{42/44}$ intensity/cell ($p < 0.05$; Figures 6A and 6B) and a higher number of $c\text{-}Fos^{+}$ cells ($p < 0.001$; Figures 6A and 6B) were observed in the DLS of 6-OHDA iMSN-D2RKO mice as compared to 6-OHDA WT controls (Figures 6A and 6B), mirroring the increase of the AIMs score (Figures 4A–4D) in these mutants. Thus, the intensity of ERK phosphorylation per cell correlates well with LID severity (Santini et al., 2007) and appears modulated by D2R signaling.

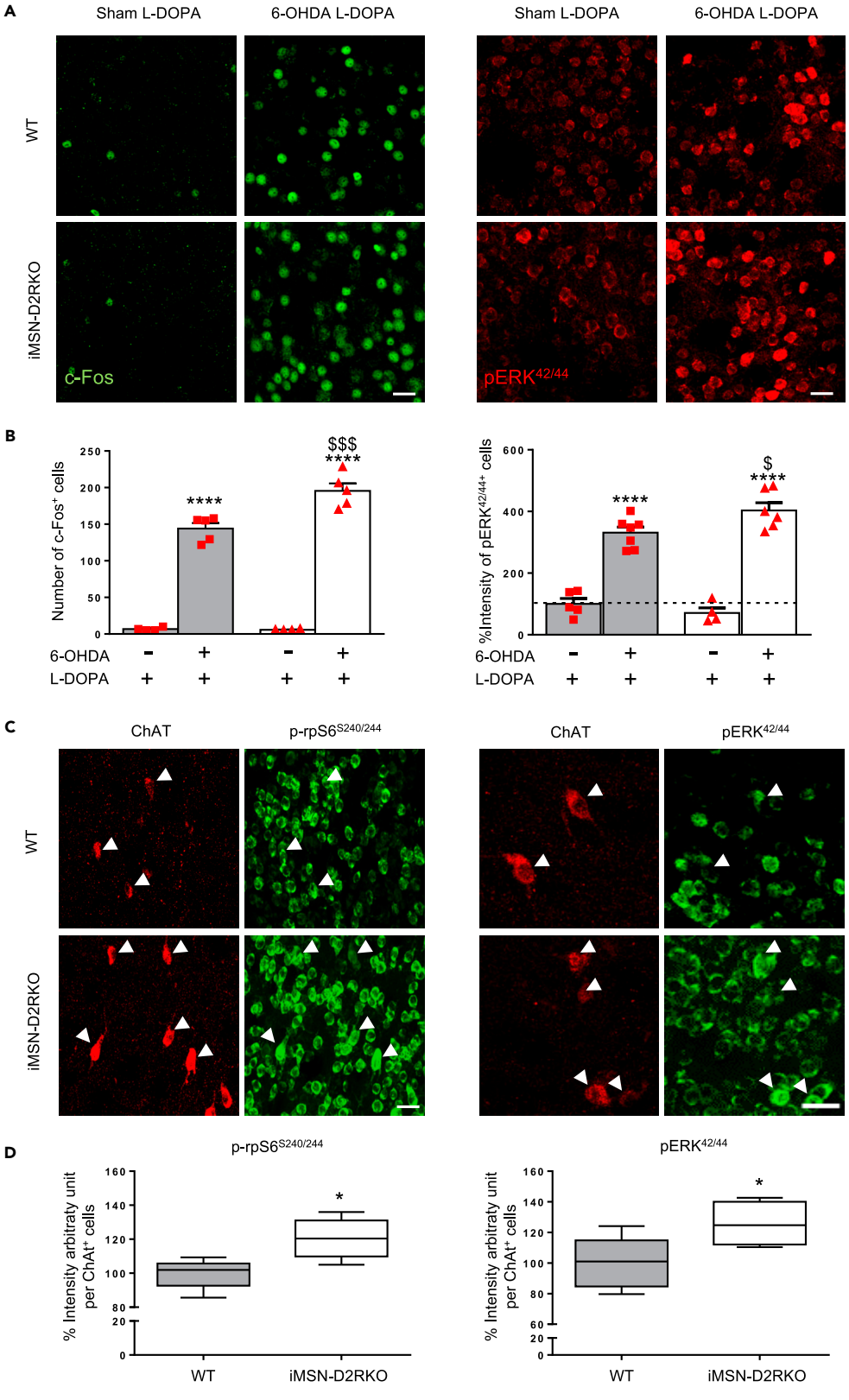
A
Sham L-DOPA
6-OHDA L-DOPA
Sham L-DOPA
6-OHDA L-DOPA
WT
iMSN-D2RKO
c-Fos
pERK42/44
B
Number of c-Fos+ cells
%Intensity of pERK42/44+ cells
$$$
****
$
6-OHDA
L-DOPA
C
ChAT
p-rpS6S240/244
ChAT
pERK42/44
WT
iMSN-D2RKO
D
p-rpS6S240/244
pERK42/44
% Intensity arbitraty unit per ChAt+ cells
WT
iMSN-D2RKO

Figure 6. Lack of D2R signaling in iMSNs enhances dMSN and ChI activity following chronic L-DOPA

(A) Representative IF images of DLS showing c-Fos^{+} (green) and pERK$^{42/44+}$ (red) cells in sham and 6-OHDA WT and iMSN-D2RKO mice following chronic L-DOPA.

(B) Bar graphs showing: (left) the total number of c-Fos^{+} cells (N = 4-5/group), and (right) the mean intensity/cell of pERK$^{42/44+}$ cells expressed as percentage of sham WT (N = 4-7/group). ****p < 0.0001 vs sham of same genotype; $ p < 0.05, $$$ p < 0.001 vs 6-OHDA WT. 2way ANOVA followed by Newman-Keuls post-hoc analysis. For c-Fos, the 2way ANOVA is significant × genotype p = 0.0117 (F (1, 14) = 8.407), × lesion p < 0.0001 (F (1, 14) = 349.1), and genotype × lesion p = 0.0098 (F (1, 14) = 8.912). For pERK$^{42/44}$, the 2way ANOVA is significant × lesion p < 0.0001 (F (1, 18) = 174.6), and genotype × lesion p = 0.0288 (F (1, 18) = 5.650).

(C) Representative IF images of DLS showing p-rpS6-S$^{240-244}$ (left, green) and pERK$^{42/44}$ (right, green) immunoreactivity in ChAT^{+} cholinergic interneurons (red) in 6-OHDA WT and iMSN-D2RKO mice following chronic L-DOPA.

(D) Left: Box plot showing the mean intensity/cell (arbitrary unit) of p-rpS6-S$^{240/244}$ immunoreactivity in ChAT^{+} cholinergic interneurons (N = 5/group). *p < 0.05 vs WT. Two-tailed t-test (t = 3.181, df = 8); (D) Right: Box plot showing the mean intensity/cell (arbitrary unit) of pERK$^{42/44}$ immunoreactivity in ChAT^{+} cholinergic interneurons (N = 5/group). *p < 0.05 vs WT. Two-tailed t-test (t = 2.402, df = 8). Data are normalized to WT and expressed as percentage. Scale bar 50 μm. See also Figures S5 and S6.

Effect of chronic L-DOPA on striatal cholinergic interneurons activity

How D2R signaling in iMSNs impact the dMSNs response to L-DOPA? Intrastriatal ACh plays a pivotal role in the regulation of MSNs activity (Lewis et al., 2020; Tanimura et al., 2018) and LID expression (Ding et al., 2011; Won et al., 2014). Thus, we asked whether the cell-specific ablation of D2R in iMSNs might affect ChIs upon L-DOPA administration to 6-OHDA lesioned animals. Activation of ChIs was evaluated in both genotypes by performing double immunofluorescence experiments using antibodies directed against choline acetyltransferase (ChAT), an exclusive marker of ChIs, and either pERK$^{42/44}$ (Ding et al., 2011) or p-rpS6-S$^{240/244}$ (Bertran-Gonzalez et al., 2012; Castello et al., 2020) as markers of signaling activation and reactivity of these neurons to L-DOPA administration. Acute L-DOPA did not activate pERK$^{42/44}$ in ChIs (Figure S6). Conversely, chronic L-DOPA induced a potent increase of pERK$^{42/44}$ as well as of p-rpS6-S$^{240/244}$ immunoreactivity in ChIs located in the DLS of WT and iMSN-D2RKO mice (Figures 6C and 6D). Interestingly, the quantification of the intensity/cell showed a statistically significant enhancement of pERK$^{42/44}$ and p-rpS6-S$^{240/244}$ immunoreactivity in the ChIs of iMSN-D2RKO mice as compared to WT mice (Figure 6C and 6D; p < 0.05). Thus, loss of D2R in iMSNs results in sustained activation of signaling in ChIs upon chronic L-DOPA treatment.

Modulation of acetylcholine signaling drastically reduces levodopa-induced dyskinesia severity in wild-type mice

DA and ACh oppositely modulate MSNs activity by stimulating postsynaptic D1R, M1R and M4R on dMSNs, and D2R and M1R on iMSNs. In PD, the striatal ACh/DA ratio is profoundly altered owing to the degeneration of nigrostriatal neurons (Fox, 2013) contributing to the generation of PD symptoms and, upon treatment, to LID (McKinley et al., 2019; Won et al., 2014).To analyze whether the unopposed M1R activation of the iMSNs in iMSN-D2RKO mice might contribute to their higher AIMs expression following L-DOPA treatment, we analyzed the anti-dyskinetic effects of VU0255035, a specific M1R antagonist, in dyskinetic WT and iMSN-D2RKO mice.

Dyskinetic iMSN-D2RKO mice were administered VU0255035 in combination with L-DOPA, then the ALO AIMs score assessed and compared to that of mice receiving exclusively L-DOPA. Following VU0255035, we observed a significant reduction of the ALO AIMs score, as compared to iMSN-D2RKO, treated only with L-DOPA (Figure S7A); importantly, AIMs intensity became comparable to that observed in L-DOPA-treated WT mice. On the other hand, VU0255035 produced only a minimal anti-dyskinetic effect in WT mice (Figure S7A).

These results suggest that ACh signaling to iMSNs exacerbates LID in the absence of D2R in these neurons, likely by potentiating the indirect pathway. They also suggest that in the WT the L-DOPA-mediated stimulation of D2R is able to counteract M1R stimulation, thus rendering the anti-dyskinetic effects of VU0255035 null.

In support of our hypothesis, we tested LFS-induced LTD in DLS coronal striatal slices from sham and 6-OHDA WT and iMSN-D2RKO mice, previously bath-exposed to the selective M1R antagonist VU0255035. Bath-application of VU0255035 induced the expression of a robust LFS-LTD in the 6-OHDA

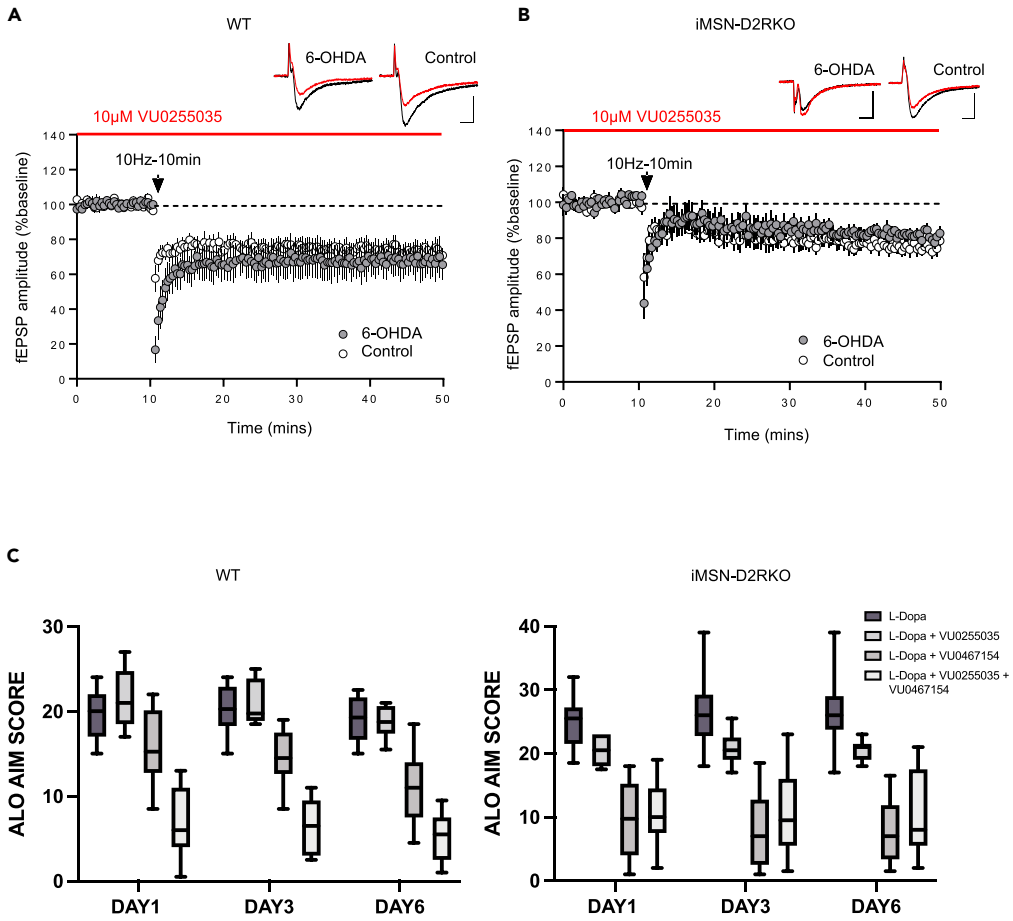

Figure 7. Reduced LID severity in WT mice treated with the co-administration of M1R antagonist and M4R allosteric modulator

Graphs showing striatal field potential recordings from LFS-LTD in coronal striatal slices from sham and 6-OHDA WT (A) and iMSN-D2RKO mice (B), previously bath exposed to the selective M1 antagonist VU 0255035. fEPSP is normalized to baseline, averaged (mean ± SEM), and plotted as a function of time. Inset: representative baseline traces in black and 40 min post-LFS in red. Bar scale; 0.4 mV/5ms.

C) ALO AIM score evaluation of WT and iMSN-D2RKO mice after five days of L-DOPA treatment (15 mg/kg) to induce dyskinesia, ten days of washout, and six days of treatment with L-DOPA 6 mg/kg, alone or in association with VU0467154 (10 mg/Kg) and/or VU0255035 (15mg/Kg). ALO AIM score was evaluated on day 1, 3, and 6 of treatment. The 2way ANOVA for WT mice is significant × time $p = 0.021$ ($F(1.782, 61.47) = 7.293$), × treatment $p < 0.0001$ ($F(3, 35) = 73.91$). The 2way ANOVA for iMSN-D2RKO mice is significant × treatment $p < 0.0001$ ($F(3, 49) = 47.06$). Data are expressed as mean values ± SEM. See also Table S2.

lesioned striatum of WT mice, reaching values comparable to that obtained from the control side (WT: control, 67% ± 9.9%, $p < 0.05$; 6-OHDA, 74% ± 4.9%, $p < 0.05$; rmANOVA: surgery × time interaction, $F_{149, 1490} = 1.389$, $p = 0.002$; Figure 7A). Importantly, the selective inhibition of M1R restored the LFS-LTD in both control and 6-OHDA-lesioned side of iMSN-D2RKO DLS (iMSN-D2RKO: control, 78% ± 4.1%, $p < 0.05$; 6-OHDA, 84% ± 3.1%, $p < 0.05$; rmANOVA: surgery × time interaction, $F_{149, 894} = 0.865$, $p = 0.86$; Figure 7B). Thus, ACh activation of M1R is critically involved in the intensity of dyskinesia.

Dopamine-mediated modulation of acetylcholine signaling in Parkinson's disease

Based on previous evidence showing that the positive allosteric modulator (PAM) of M4R (VU0467154) significantly counteract the pro-dyskinetic effects of L-DOPA (Shen et al., 2015), we asked whether the combined blockade of M1R and positive modulation of M4R would further ameliorate AIMs in dyskinetic WT and iMSN-D2RKO mice.

To do this, dyskinetic WT and iMSN-D2RKO mice received a sub-chronic administration of L-DOPA (6 mg/kg, s.c.) plus benserazide (12 mg/kg, s.c.) alone or in association with the M1R antagonist VU0255035 (15 mg/kg; i.p.), and/or with the M4R PAM VU0467154 (10 mg/kg; i.p). ALO AIM scores were evaluated on day 1, 3, and 6 of the treatment (Figure 7C). Chronic treatment with VU0255035 showed a statistically significant reduction of AIMs only in the iMSN-D2RKO mice with the best performance at day 6 ($p < 0.001$, Figure 7C). VU0467154 alone significantly reduced AIMs in iMSN-D2RKO mice from day 1, likely by partially balancing the activity of the output striatal pathways ($p < 0.0001$, Figure 7C). In WT mice, VU0467154 significantly reduced the pro-dyskinetic effects of L-DOPA starting from day 3 ($p < 0.01$, Figure 7C); however, this reduction was not as accentuated as that of the combination of muscarinic agents ($p < 0.0001$, Figure 7C). Indeed, both genotypes receiving L-DOPA in combination with VU0255035 and VU0467154, showed a strong reduction of ALO AIMs starting from day 1, with the highest anti-dyskinetic effect observed on day 6 in both genotypes ($p < 0.0001$, Figure 7C). The 2way ANOVA for WT mice is significant × Time $p = 0.021$ $F(1.782, 61.47) = 7.293$, × Treatment $p < 0.0001$ $F(3, 35) = 73.91$. The 2way ANOVA for iMSN-D2RKO mice is significant × Treatment $p < 0.0001$ $F(3, 49) = 47.06$. Statistical results of Bonferroni's multiple comparisons test are shown in Table S2. These results indicate the importance of restoring a balanced DA/ACh signaling within the DA-deprived striatum to reduce LID, as demonstrated by the superior anti-dyskinetic effects of the combination of VU0255035 and VU0467154 in mice.

DISCUSSION

Loss of dopaminergic neurons, and the consequent reduction of dopamine signaling, are at the basis of PD. Surprisingly, the constitutive loss of D1R is not detrimental to locomotion (Xu et al., 1994), although the dyskinetic effects of L-DOPA are no longer observed in D1RKO mice (Darmopil et al., 2009). Conversely, genetically engineered mice lacking D2R either constitutively or in a cell-specific fashion only in iMSNs, show that the absence of D2R signaling is largely involved in the loss of coordination and reduced movements characteristic of PD (Anzalone et al., 2012; Baik et al., 1995; Kharkwal et al., 2016; Lemos et al., 2016). These results agree with the L-DOPA-mediated activation of the MSNs-derived pathways to the SNr and GPi (Cenci and Konradi, 2010), and indicate that loss of D2R signaling in iMSNs results in unbalanced signaling to extrastriatal, but also intrastriatal, circuits (Lemos et al., 2016; Kharkwal et al., 2016).

While L-DOPA stimulation of D1R signaling in dMSNs in LID is well established (Cenci, M.A., and Konradi), that of D2R signaling in iMSNs, although involved, is less well defined. This because D2R is widely expressed in the striatum not only on iMSNs, but also on ChIs, as well as on dopaminergic and cortical afferents; all these neurons are intertwined in complex circuits that are still to be clarified.

This study aimed at analyzing how and whether the lack of D2Rs selectively in iMSNs affects LID. This approach differs from that of others that have previously analyzed the involvement of iMSNs in LID (Alcacer et al., 2017; Girasole et al., 2018) in which D2R expressing iMSNs were manipulated as a whole. Similarly, using pharmacological approaches a clear participation of D2R/D3R signaling was assessed (Drake et al., 2013; Rascol et al., 2006; Sebastianutto et al., 2016) but the cell types involved in it were not clarified. Using constitutive knockout of D2Rs in mice it was shown that the total loss of D2R signaling had no effects in L-DOPA-treated dyskinetic mice (Darmopil et al., 2009).

These apparent discrepancies are interesting as they support and confirm that D2R signaling in the striatum affects a majority of cell types and that it is this complexity that has prevented a full knowledge of the D2R implication in LID more than lack of D2R ligands capable of completely distinguish between D2R and D3R (Lanza et al., 2021; Solís et al., 2017).

In this study, using 6-OHDA lesioned iMSN-D2RKO and WT mice, we observed a lower reduction of the total motor activity and of the turning behavior as compared to WT mice. In agreement with the notion that synaptic plasticity dysfunctions are critically involved in the emergence of motor impairment (Schroll et al., 2014), we found that the removal of D2R in iMSN was sufficient to prevent the expression of LFS-induced LTD in striatal slices from sham iMSN-D2RKO mice, in a manner similar to WT mice having lost dopaminergic neurons after 6-OHDA lesion (Picconi et al., 2003; Thiele et al., 2014). These results support previous studies suggesting that the DA stimulation of D2R in iMSNs is required for endocannabinoids production and, subsequently, for the stimulation of presynaptic Cannabinoid receptor type 1 (Kreitzer and Malenka, 2005, 2007).

High-frequency stimulation (HFS)-LTD deficiency has also been reported in another mouse model, in which to delete D2Rs in iMSNs, the Cre-recombinase was under the control of the Adenosine A2a promoter (Augustin et al., 2018). In this study, HFS-LTD deficiency was observed using whole-cell patch clamp recording from iMSNs, but not in field potential recordings. As the expression of LFS-LTD and HFS-LTD depends on the involvement of different intracellular mechanisms (Ronesi and Lovinger, 2005), we hypothesize that these discrepancies may be partially related to the different electrical stimulation protocols used.

Comparisons of the transcriptomes of the DLS from WT and iMSN-D2RKO mice undergoing sham or 6-OHDA lesions with or without L-DOPA treatment, enabled us to obtain the footprint of lack of D2R signaling in iMSNs. This analysis is the first to be done in a cell-type specific iMSN-D2R mutants. Importantly, we observed that, already in sham conditions, there is a striking upregulation of the LRRK2 gene in the absence of D2R in iMSNs. Mutations in LRRK2 have been identified in familial and sporadic PD; furthermore, LRRK2 overexpression has been shown to be detrimental to neuron's physiology (Jeong and Lee, 2020) indicating that D2R signaling is a critical element in the control of the expression of this kinase. Future studies will be aimed at investigating whether LRRK2 overexpression in iMSN-D2RKO mice might be caused by a direct D2R-dependent inhibition of its expression in iMSNs or indirect, in dMSNs or other striatal neurons.

KEGG analyses of the differentially expressed genes showed significant changes in members of the cAMP and calcium signaling pathways underlining the important regulation by D2R in iMSNs on striatal gene expression (de Gortari and Mengod, 2010; Gresack et al., 2014). Indeed, differentially expressed genes identified by comparing sham WT to sham iMSN-D2RKO DLS were all up-regulated in the absence of D2R in iMSN-D2RKO mice, with some of them previously linked to PD (Morales-Garcia et al., 2011; Nicolini et al., 2015; Park et al., 2014; Wennogle et al., 2017). Thus, it might be concluded that D2R signaling in iMSNs exerts a global negative control upon striatal genes' expression and it acts as an inhibitory filter of striatal functions affecting dMSNs and striatal output pathways (Cai et al., 2021; Kharkwal et al., 2016; Lemos et al., 2016; McKinley et al., 2019).

The significant changes at the gene expression level observed by loss of D2R signaling in the iMSNs parallel the bradikynesia and altered the coordination of iMSN-D2RKO mice (Anzalone et al., 2012). In this respect, the bradykinesia observed in iMSN-D2RKO mice originates from the hyper-GABAergic tone generated by collateral projections coming from iMSNs and directed to dMSNs, rather than from the iMSNs output target (Lemos et al., 2016). Interestingly, in line with the importance of D2R signaling in iMSNs on intrastriatal gene expression, while members of the cAMP pathway are up-regulated in the DLS of iMSN-D2RKO in basal conditions, in the WT, members of this same pathway are instead down-regulated following 6-OHDA lesion. These results imply that in basal conditions DA through D2R signaling inhibits these genes expression; they also show the absence of mechanisms activated either by different members of the dopaminergic system or by other intrastriatal circuits to compensate for the absence of D2R in these neurons.

DA depletion induced by either 6-OHDA or reserpine dramatically reduces the number and strength of MSNs collaterals (Taverna et al., 2008). Thus, we hypothesized an amplification of this condition in iMSN-D2RKO mice following chronic L-DOPA treatment in 6-OHDA lesioned mutants. Indeed, iMSN-D2RKO mice showed a higher degree and intensity of AIMs in comparison to WT mice.

Interestingly, while in WT mice chronic L-DOPA treatment re-established the expression of DEGs in 6-OHDA lesioned animals to basal levels, in 6-OHDA lesioned iMSN-D2RKO mice it had only a minimal effect. Thus, in the absence of D2R signaling in iMSN, L-DOPA-mediated stimulation of dMSNs is not sufficient to restore gene expression to the basal conditions. This observation is further enhanced by quantifications of c-Fos and pERK immunoreactivity which was significantly stronger in the DLS of D2R mutants as compared to the WT following L-DOPA treatment, mirroring the increased elevation of genes' expression in the cAMP pathway of iMSN-D2RKO DLS. For instance, overexpression of ADCY5 is not overturned upon L-DOPA treatment of iMSN-D2RKO lesioned mice leading to the potent up-regulation of downstream genes associated with LID, such as c-fos.

The cholinergic system is also critically involved in the striatal regulation of the cAMP pathway (Migeon and Nathanson, 1994), and acetylcholine signaling to MSNs is implicated in LID (Ding et al., 2011; Shen et al., 2015; Won et al., 2014). Reduced DA as well as chronic L-DOPA treatment strongly affects the appropriate

control of ACh release and the activity of striatal cholinergic interneurons (Cai et al., 2021; McKinley et al., 2019). In this respect, we found that the immunoreactivity of pERK and p-rpS6-S240/244 was significatively elevated in L-DOPA-treated iMSN-D2RKO mice as compared to WT mice, thus indicating a sustained activation of ChIs in our mutants. We hypothesized that the unopposed stimulation of muscarinic M1Rs in iMSNs in the absence of D2R might synergize with weakened MSNs collaterals and underlie the stronger LID observed in iMSN-D2RKO mice. Indeed, blocking M1R using the specific antagonist VU0255035 reduced the intensity of dyskinesia of iMSN-D2RKO mice to WT levels.

On the contrary, the M1R antagonist did not improve AIMs in WT mice showing that the anti-dyskinetic effect of M1R is contained in the presence of D2R signaling. Nonetheless, VU0255035 restored LFS-LTD in both genotypes. Interestingly, in experiments conducted in iMSN-D2RKO mice, both the control and the lesioned side appeared equally responding to VU0255035 suggesting that in both conditions LFS-LTD can be restored by blocking M1R (Wang et al., 2006).

The muscarinic M4R has also been implicated in LID (Shen et al., 2015). Interestingly, RNA-seq data showed a marked change of M4R expression in sham iMSN-D2RKO mice compared with WT, as well as in both genotypes following DA depletion. Considering this evidence and the positive results obtained by M1R blockade in iMSN-D2RKO, we tested the antidyskinetic effects generated by the pharmacological manipulation of M1 and M4 muscarinic receptors in WT mice. Our results show an outstanding synergistic effect on LID by targeting these two receptors, followed by a drastic reduction of the AIM score. These treatments were also efficient in reducing LID in iMSN-D2RKO mice. Thus, loss of DA in PD alters the activity of MSNs and participates to the appearance of dyskinetic movements by affecting striatal cholinergic signaling.

In conclusion, our results illustrate the prominent role of D2R in iMSNs in the regulation of motor activity and development of LID following chronic L-DOPA. The identification of genes whose expression is altered under the different conditions used, allowed us to observe that loss of D2R signaling has a big impact on striatal gene expression affecting pathways previously involved in PD. Importantly, our studies show that D2R signaling is required for maintaining the expression of members of specific pathways under control and in its absence the resulting up-regulation is detrimental to the physiological characteristics of striatal neurons and to behavior. KEGG analyses performed after 6-OHDA lesions in both genotypes showed opposing pathways activated in the absence of D2Rs in iMSNs. In the WT, a larger number of genes belonged to gabaergic signaling while in IMSN-D2RKO mice to the glutamatergic. It is tempting to speculate that the absence of D2R signaling in iMSNs might change the direction of neuronal plasticity in striatal circuits, in agreement with previous reports (Calabresi et al., 1997).

Importantly, we show that in the absence of D2R in iMSNs the unopposed M1R signaling is responsible for the increased dyskinesia of iMSN-D2RKO mice. We speculate that the pulsatile control of L-DOPA on iMSNs and cholinergic interneurons does not allow the proper cholinergic control of MSNs leading to LID.

Thus, our study using mice with a selective deletion of D2R in iMSNs, extends and complements previous studies by demonstrating that absence of D2R signaling specifically in iMSNs has a preponderant role in the control of gene expression and the pathophysiology of PD through the alteration of striatal circuits.

Limitations of the study

Electrophysiological analyses from striatal slices did not allow us to evaluate responses of different neuronal populations at the single-cell level and were restricted to the evaluation of LFS-induced LTD, the best characterized and reproducible form of long-term plasticity in these synapses (Kreitzer and Malenka, 2005). Nevertheless, it is known that in the healthy striatum both iMSNs and dMSNs may also express another major form of corticostriatal plasticity known as long-term potentiation (LTP), which strengthens the connections between cortical and striatal neurons. Considering our observation indicating a major role of D2R in iMSNs in the inhibition of intrastriatal circuits, further studies are needed to investigate whether D2R in iMSNs may affect the expression of LTP in MSNs both in PD and LID.

A functional characterization of GABAergic MSNs collaterals following DA-depletion and L-DOPA treatment would be suited. Loss of D2R signaling in iMSNs results in increased GABA-mediated inhibition of dMSN activity (Kharkwal et al., 2016; Lemos et al., 2016), the understanding of how the activity of MSNs collaterals may affect intrastriatal circuits in PD and LID will be fundamental to fully clarify the mechanisms leading to the behavioral and molecular responses observed in our mice.

Here, we performed bulk RNA-seq of the DLS of WT and iMSN-D2RKO mice. Single cells RNA-seq will help assign the variation of gene expression to identified neuronal populations.

STAR★METHODS

Detailed methods are provided in the online version of this paper and include the following:

- KEY RESOURCES TABLE
- RESOURCE AVAILABILITY
  - Lead contact
  - Materials availability
  - Data and code availability
- EXPERIMENTAL MODEL AND SUBJECT DETAILS
- METHOD DETAILS
  - Chemical and reagents
  - Unilateral 6-OHDA stereotaxic surgery
  - Behavioral analyses
  - Abnormal involuntary movements evaluation
  - Experimental Plan
  - Immunofluorescence
  - Western blot
  - RNA preparation for RNA-sequencing
  - Library preparation for RNA-Sequencing
  - Bioinformatics
  - Field Potential Recordings
- QUANTIFICATION AND STATISTICAL ANALYSIS

SUPPLEMENTAL INFORMATION

Supplemental information can be found online at https://doi.org/10.1016/j.isci.2022.105263.

ACKNOWLEDGMENTS

We thank all the members of the lab for the scientific discussion and technical assistance. We acknowledge Melanie Oakes and Seung-Ah Chung for support in RNA-seq analyses. We thank Dr. Christopher D. Vanderwal for help synthetizing the M1R antagonist (VU0255035). E. Florio was supported by the "Fondazione Sebastiano e Rita Raeli," from the University of Rome, "Torvergata." M. Serra was supported by the Sardinia Regional Government (P.O.R. Sardegna F.S.E.-Operational Program of the Autonomous Region of Sardinia, European Social Fund 2014-2020). This work was supported by the Institut National de la Santé et de la Recherche Médicale (Inserm) IR-PG11787 (445135-49125).

AUTHOR CONTRIBUTIONS

EF and MS performed surgeries, pharmacological and behavioral experiments. EF performed bioinformatics. EF and RGL performed Western blots. MS performed immunofluorescence analyses. EK and MW performed Field Potential Recordings and analyses. MF synthesized the M1R antagonist compound (VU0255035). EF, MS, RGL, MM, and EB designed the study and analyzed the data. EF, MS, and EB wrote the article.

DECLARATION OF INTERESTS

The authors declare no competing interests.

INCLUSION AND DIVERSITY

We support inclusive, diverse, and equitable conduct of research.

Received: June 8, 2022
Revised: July 19, 2022
Accepted: September 25, 2022
Published: October 21, 2022

REFERENCES

Aizman, O., Brismar, H., Uhlén, P., Zettergren, E., Levey, A.I., Forssberg, H., Greengard, P., and Aperia, A. (2000). Anatomical and physiological evidence for D1 and D2 dopamine receptor colocalization in neostriatal neurons. Nat. Neurosci. *3*, 226–230. https://doi.org/10.1038/72929.

Albin, R.L., Young, A.B., and Penney, J.B. (1989). The functional anatomy of basal ganglia disorders. Trends Neurosci *12*, 366–375. https://doi.org/10.1016/0166-2236(89)90074-X-.

Alcacer, C., Andreoli, L., Sebastianutto, I., Jakobsson, J., Fieblinger, T., and Cenci, M.A. (2017). Chemogenetic stimulation of striatal projection neurons modulates responses to Parkinson's disease therapy. J. Clin. Invest. *127*, 720–734. https://doi.org/10.1172/JCI90132.

Alexander, G.E., and Crutcher, M.D. (1990). Functional architecture of basal ganglia circuits:neural substrates of parallel processing. Trends Neurosci. *13*, 266–271. https://doi.org/10.1016/0166-2236(90)90107-l.

Anzalone, A., Lizardi-Ortiz, J.E., Ramos, M., De Mei, C., Hopf, F.W., Iaccarino, C., Halbout, B., Jacobsen, J., Kinoshita, C., Welter, M., et al. (2012). Dual control of dopamine synthesis and release by presynaptic and postsynaptic dopamine D2 receptors. J. Neurosci. *32*, 9023–9034. https://doi.org/10.1523/JNEUROSCI.0918-12.2012.

Augustin, S.M., Chancey, J.H., and Lovinger, D.M. (2018). Dual dopaminergic regulation of corticostriatal plasticity by cholinergic interneurons and indirect pathway medium spiny neurons. Cell Rep. *11*, 2883–2893. https://doi.org/10.1016/j.celrep.2018.08.042.

Baik, J.H., Picetti, R., Saiardi, A., Thiriet, G., Dierich, A., Depaulis, A., Le Meur, M., and Borrelli, E. (1995). Parkinsonian-like locomotor impairment in mice lacking dopamine D2 receptors. Nature *377*, 424–428. https://doi.org/10.1038/377424a0.

Bastide, M.F., Meissner, W.G., Picconi, B., Fasano, S., Fernagut, P.O., Feyder, M., Francardo, V., Alcacer, C., Ding, Y., Brambilla, R., et al. (2015). Progress in Neurobiology Pathophysiology of L-dopa-induced motor and non-motor complications in Parkinson' s disease. Prog. Neurobiol. *132*, 96–168. https://doi.org/10.1016/j.pneurobio.2015.07.002.

Bertran-Gonzalez, J., Chieng, B.C., Laurent, V., Valjent, E., and Balleine, B.W. (2012). Striatal cholinergic interneurons display activity-related phosphorylation of ribosomal protein S6. PLoS One *7*, e53195. https://doi.org/10.1371/journal.pone.0053195.

Bido, S., Marti, M., and Morari, M. (2011). Amantadine attenuates levodopa-induced dyskinesia in mice and rats preventing the accompanying rise in nigral GABA levels. J. Neurochem. *118*, 1043–1055. https://doi.org/10.1111/j.1471-4159.2011.07376.x.

Cai, Y., Nielsen, B.E., Boxer, E.E., Aoto, J., and Ford, C.P. (2021). Loss of nigral excitation of cholinergic interneurons contributes to parkinsonian motor impairments. Neuron *109*, 1137–1149.e5. https://doi.org/10.1016/j.neuron.2021.01.028.

Calabresi, P., Saiardi, A., Pisani, A., Baik, J.-H., Centonze, D., Mercuri, N.B., Bernardi, G., and Borrelli, E. (1997). Abnormal synaptic plasticity in the striatum of mice lacking dopamine D2 receptors. J. Neurosci. *17*, 4536–4544. https://doi.org/10.1523/JNEUROSCI.17-12-04536.1997.

Castello, J., Cortés, M., Malave, L., Kottmann, A., Sibley, D.R., Friedman, E., and Rebholz, H. (2020). The Dopamine D5 receptor contributes to activation of cholinergic interneurons during L-DOPA induced dyskinesia. Sci. Rep. *10*, 4974. https://doi.org/10.1038/s41598-020-61832-3.

Cenci, M.A., and Crossman, A.R. (2018). Animal models of l-dopa-induced dyskinesia in Parkinson's disease. Mov. Disord. *33*, 889–899. https://doi.org/10.1002/mds.27337.

Cenci, M.A., and Konradi, C. (2010). Maladaptive striatal plasticity in l-DOPA-induced dyskinesia. Prog. Brain Res. *183*, 209–233. https://doi.org/10.1016/S0079-6123(10)83011-0.

Chen, E.Y., Tan, C.M., Kou, Y., Duan, Q., Wang, Z., Meirelles, G.V., Clark, N.R., and Ma'ayan, A. (2013). Enrichr: interactive and collaborative HTML5 gene list enrichment analysis tool. BMC Bioinf. *14*. https://doi.org/10.1186/1471-2105-14-128.

Cortés, M., Malave, L., Castello, J., Flajolet, M., Cenci, M.A., Friedman, E., and Rebholz, H. (2017). CK2 oppositely modulates L-DOPA-induced dyskinesia via striatal projection neurons expressing D1 or D2 receptors. J. Neurosci. *37*, 11930–11946. https://doi.org/10.1523/JNEUROSCI.0443-17.2017.

Darmopil, S., Martín, A.B., De Diego, I.R., Ares, S., and Moratalla, R. (2009). Genetic inactivation of dopamine D1 but not D2 receptors inhibits L-DOPA-induced dyskinesia and histone activation. Biol. Psychiatry. *66*, 603–613. https://doi.org/10.1016/j.biopsych.2009.04.025.

de Gortari, P., and Mengod, G. (2010). Dopamine D1, D2 and mu-opioid receptors are co-expressed with adenylyl cyclase 5 and phosphodiesterase 7B mRNAs in striatal rat cells. Brain Res. *1310*, 37–45. https://doi.org/10.1016/j.brainres.2009.11.009.

De Deurwaerdère, P., Di Giovanni, G., and Millan, M.J. (2017). Progress in Neurobiology Expanding the repertoire of L-DOPA's actions: a comprehensive review of its functional neurochemistry. Prog. Neurobiol. *151*, 57–100. https://doi.org/10.1016/j.pneurobio.2016.07.002.

Ding, Y., Won, L., Britt, J.P., Lim, S.A.O., McGehee, D.S., and Kang, U.J. (2011). Enhanced striatal cholinergic neuronal activity mediates L-DOPA-induced dyskinesia in parkinsonian mice. Proc. Natl. Acad. Sci. USA *108*, 840–845. https://doi.org/10.1073/pnas.1006511108.

Dobbs, L.K., Kaplan, A.R., Lemos, J.C., Matsui, A., Rubinstein, M., and Alvarez, V.A. (2016). Dopamine regulation of lateral inhibition between striatal neurons gates the stimulant actions of cocaine. Neuron *90*, 1100–1113. https://doi.org/10.1016/j.neuron.2016.04.031.

Drake, J.D., Kibuuka, L.N., Dimitrov, K.D., and Pollack, A.E. (2013). Abnormal involuntary movement (AIM) expression following D2 dopamine agonist challenge is determined by the nature of prior dopamine receptor stimulation (priming) in 6-hydroxydopamine lesioned rats. Pharmacol. Biochem. Behav. *105*, 26–33. https://doi.org/10.1016/j.pbb.2013.01.014.

Fasano, S., Bezard, E., D'Antoni, A., Francardo, V., Indrigo, M., Qin, L., Doveró, S., Cerovic, M., Cenci, M.A., and Brambilla, R. (2010). Inhibition of Ras-guanine nucleotide-releasing factor 1 (Ras-GRF1) signaling in the striatum reverts motor symptoms associated with L-dopa-induced dyskinesia. Proc. Natl. Acad. Sci. USA *107*, 21824–21829. https://doi.org/10.1073/pnas.1012071107.

Fox, H.S. (2013). Non-dopaminergic treatments for motor control in Parkinson's Disease. Drugs *73*, 1405–1415. https://doi.org/10.1007/s40265-013-0105-4.

Francardo, V., Recchia, A., Popovic, N., Andersson, D., Nissbrandt, H., and Cenci, M.A. (2011). Impact of the lesion procedure on the profiles of motor impairment and molecular responsiveness to L-DOPA in the 6-hydroxydopamine mouse model of Parkinson's disease. Neurobiol. Dis. *42*, 327–340. https://doi.org/10.1016/j.nbd.2011.01.024.

Gerfen, C.R., and Surmeier, D.J. (2011). Modulation of striatal projection systems by dopamine. Annu. Rev. Neurosci. *34*, 441–466. https://doi.org/10.1146/annurev-neuro-061010-113641.

Girasole, A.E., Lum, M.Y., Nathaniel, D., Bair-Marshall, C.J., Guenthner, C.J., Luo, L., Kreitzer, A.C., and Nelson, A.B. (2018). A subpopulation of striatal neurons mediates levodopa-induced dyskinesia. Neuron *97*, 787–795.e6. https://doi.org/10.1016/j.neuron.2018.01.017.

Goto, S. (2017). Striatal gαolf/cAMP signal-dependent mechanism to generate levodopa-induced dyskinesia in Parkinson's disease. Front. Cell. Neurosci. *11*, 364. https://doi.org/10.3389/fncel.2017.00364.

Gresack, J.E., Seymour, P.A., Schmidt, C.J., and Risbrough, V.B. (2014). Inhibition of phosphodiesterase 10A has differential effects on dopamine D1 and D2 receptor modulation of sensorimotor gating. Psychopharmacology *231*, 2189–2197. https://doi.org/10.1007/s00213-013-3371-7.

Ho, H., Both, M.D., Siniard, A., Sharma, S., Notwell, J.H., Wallace, M., Leone, D.P., Nguyen, A., Zhao, E., Lee, H., et al. (2018). A guide to single-cell transcriptomics in adult rodent brain: the medium spiny neuron transcriptome revisited. Front. Cell. Neurosci. *12*, 159. https://doi.org/10.3389/fncel.2018.00159.

Jeong, G.R., and Lee, B.D. (2020). Pathological functions of LRRK2 in Parkinson's disease. Cells *9*, 2565. https://doi.org/10.3390/cells9122565.

Jiang, M., Spicher, K., Boulay, G., Wang, Y., and Birnbaumer, L. (2001). Most central nervous system D2 dopamine receptors are coupled to their effectors by Go. Proc. Natl. Acad. Sci. USA *98*, 3577–3582. https://doi.org/10.1073/pnas.051632598.

Kharkwal, G., Radl, D., Lewis, R., and Borrelli, E. (2016). Dopamine D2 receptors in striatal output neurons enable the psychomotor effects of cocaine. Proc. Natl. Acad. Sci. USA *113*, 11609–11614. https://doi.org/10.1073/pnas.1608362113.

Komatsu, H., Maruyama, M., Yao, S., Shinohara, T., Sakuma, K., Imaichi, S., Chikatsu, T., Kuniyeda, K., Siu, F.K., Peng, L.S., et al. (2014). Anatomical transcriptome of G protein-coupled receptors leads to the identification of a novel therapeutic candidate GPR52 for psychiatric disorders. PLoS One *9*, e90134. https://doi.org/10.1371/journal.pone.0090134.

Kreitzer, A.C., and Malenka, R.C. (2005). Dopamine modulation of state-dependent endocannabinoid release and long-term depression in the striatum. J. Neurosci. *25*, 10537–10545. https://doi.org/10.1523/JNEUROSCI.2959-05.2005.

Kreitzer, A.C., and Malenka, R.C. (2007). Endocannabinoid-mediated rescue of striatal LTD and motor deficits in Parkinson's disease models. Nature *445*, 643–647. https://doi.org/10.1038/nature05506.

Lanza, K., Centner, A., Coyle, M., Del Priore, I., Manfredsson, F.P., and Bishop, C. (2021). Genetic suppression of the dopamine D3 receptor in striatal D1 cells reduces the development of L-DOPA-induced dyskinesia. Exp. Neurol. *336*, 113534. https://doi.org/10.1016/j.expneurol.2020.113534.

Lee, J.Y., Jeon, B.S., Kim, H.J., and Park, S.S. (2012). Genetic variant of HTR2A associates with risk of impulse control and repetitive behaviors in Parkinson's disease. Parkinsonism Relat. Disord. *18*, 76–78. https://doi.org/10.1016/j.parkreldis.2011.08.009.

Lee, K.W., Hong, J.H., Choi, I.Y., Che, Y., Lee, J.K., Yang, S.D., Song, C.W., Kang, H.S., Lee, J.H., Noh, J.S., et al. (2002). Impaired D2 dopamine receptor function in mice lacking type 5 adenylyl cyclase. J. Neurosci. *22*, 7931–7940. https://doi.org/10.1523/JNEUROSCI.22-18-07931.2002.

Lemos, J.C., Friend, D.M., Kaplan, A.R., Shin, J.H., Rubinstein, M., Kravitz, A.V., and Alvarez, V.A. (2016). Enhanced GABA transmission drives bradykinesia following loss of dopamine D2 receptor signaling. Neuron *90*, 824–838. https://doi.org/10.1016/j.neuron.2016.04.040.

Lerner, T.N., and Kreitzer, A.C. (2012). RGS4 is required for dopaminergic control of striatal LTD and susceptibility to parkinsonian motor deficits. Neuron *73*, 347–359. https://doi.org/10.1016/j.neuron.2011.11.015.

Lewis, R.G., Serra, M., Radl, D., Gori, M., Tran, C., Michalak, S.E., Vanderwal, C.D., and Borrelli, E. (2020). Dopaminergic control of striatal cholinergic interneurons underlies cocaine-induced psychostimulation. Cell Rep. *31*, 107527. https://doi.org/10.1016/j.celrep.2020.107527.

Lindgren, H.S., Andersson, D.R., Lagerkvist, S., Nissbrandt, H., and Cenci, M.A. (2010). L-DOPA-induced dopamine efflux in the striatum and the substantia nigra in a rat model of Parkinson's disease: temporal and quantitative relationship to the expression of dyskinesia. J. Neurochem. *112*, 1465–1476. https://doi.org/10.1111/j.1471-4159.2009.06556.x.

Lundblad, M., Usiello, A., Carta, M., Håkansson, K., Fisone, G., and Cenci, M.A. (2005). Pharmacological validation of a mouse model of L-DOPA-induced dyskinesia. Exp. Neurol. *194*, 66–75. https://doi.org/10.1016/j.expneurol.2005.02.002.

Mandemakers, W., Snellinx, A., O'Neill, M.J., and de Strooper, B. (2012). LRRK2 expression is enriched in the striosomal compartment of mouse striatum. Neurobiol. Dis. *48*, 582–593. https://doi.org/10.1016/j.nbd.2012.07.017.

Martikainen, M.H., Päivärinta, M., Hietala, M., and Kaasinen, V. (2015). Clinical and imaging findings in Parkinson disease associated with the A53ESNCAmutation. Neurol. Genet. *1*, e27. https://doi.org/10.1212/NXG.0000000000000027.

McKinley, J.W., Shi, Z., Kawikova, I., Hur, M., Bamford, I.J., Sudarsana Devi, S.P., Vahedipour, A., Darvas, M., and Bamford, N.S. (2019). Dopamine deficiency reduces striatal cholinergic interneuron function in models of Parkinson's disease. Neuron *103*, 1056–1072.e6. https://doi.org/10.1016/j.neuron.2019.06.013.

Meissner, W., Ravenscroft, P., Reese, R., Harnack, D., Morgenstern, R., Kupsch, A., Klitgaard, H., Bioulac, B., Gross, C.E., Bezard, E., and Boraud, T. (2006). Increased slow oscillatory activity in substantia nigra pars reticulata triggers abnormal involuntary movements in the 6-OHDA-lesioned rat in the presence of excessive extracelullar striatal dopamine. Neurobiol. Dis. *22*, 586–598. https://doi.org/10.1016/j.nbd.2006.01.009.

Migeon, J.C., and Nathanson, N.M. (1994). Differential regulation of cAMP-mediated gene transcription by m1 and m4 muscarinic acetylcholine receptors. Preferential coupling of m4 receptors to Gi alpha-2. J. Biol. Chem. *1*, 9767–9773.

Morales-Garcia, J.A., Redondo, M., Alonso-Gil, S., Gil, C., Perez, C., Martinez, A., Santos, A., and Perez-Castillo, A. (2011). Phosphodiesterase 7 inhibition preserves dopaminergic neurons in cellular and rodent models of Parkinson disease. PLoS One *6*, e17240. https://doi.org/10.1371/journal.pone.0017240.

Nicolini, F., Foltynie, T., Reis Marques, T., Muhlert, N., Tziortzi, A.C., Searle, G.E., Natesan, S., Kapur, S., Rabiner, E.A., Gunn, R.N., et al. (2015). Loss of phosphodiesterase 10A expression is associated with progression and severity in Parkinson's disease. Brain *138* (Pt 10), 3003–3015. https://doi.org/10.1093/brain/awv219.

Oeckl, P., Hengerer, B., and Ferger, B. (2014). G-protein coupled receptor 6 deficiency alters striatal dopamine and cAMP concentrations and reduces dyskinesia in a mouse model of Parkinson's disease. Exp. Neurol. *257*, 1–9. https://doi.org/10.1016/j.expneurol.2014.04.010.

Park, H.Y., Kang, Y.M., Kang, Y., Park, T.S., Ryu, Y.K., Hwang, J.H., Kim, Y.H., Chung, B.H., Nam, K.H., Kim, M.R., et al. (2014). Inhibition of adenylyl cyclase type 5 prevents L-DOPA-induced dyskinesia in an animal model of Parkinson's disease. J. Neurosci. *34*, 11744–11753. https://doi.org/10.1523/JNEUROSCI.0864-14.2014.

Patricio, F., Morales-Andrade, A.A., Patricio-Martínez, A., and Limón, I.D. (2020). Cannabidiol as a therapeutic target: evidence of its neuroprotective and neuromodulatory function in Parkinson's disease. Front. Pharmacol. *11*, 595635. https://doi.org/10.3389/fphar.2020.595635.

Paxinos, G., and Franklin, K.B.J. (2001). Mouse Brain in Stereotaxic Coordinates.

Picconi, B., Centonze, D., Håkansson, K., Bernardi, G., Greengard, P., Fisone, G., Cenci, M.A., and Calabresi, P. (2003). Loss of bidirectional striatal synaptic plasticity in L-DOPA-induced dyskinesia. Nat. Neurosci. *6*, 501–506. https://doi.org/10.1038/nn1040.

Rascol, O., Brooks, D.J., Korczyn, A.D., De Deyn, P.P., Clarke, C.E., Lang, A.E., and Abdalla, M. (2006). Development of dyskinesias in a 5-year trial of ropinirole and L-dopa. Mov Disord *21*, 1844–1850. https://doi.org/10.1002/mds.20988.

Ronesi, J., and Lovinger, D.M. (2005). Induction of striatal long-term synaptic depression by moderate frequency activation of cortical afferents in rat. J. Physiol. *562*, 245–256. https://doi.org/10.1113/jphysiol.2004.068460.

Rouillard, C., Baillargeon, J., Paquet, B., St-Hilaire, M., Maheux, J., Lévesque, C., Darlix, N., Majeur, S., and Lévesque, D. (2018). Genetic disruption of the nuclear receptor Nur77 (Nr4a1) in rat reduces dopamine cell loss and l-Dopa-induced dyskinesia in experimental Parkinson's disease. Exp. Neurol. *304*, 143–153. https://doi.org/10.1016/j.expneurol.2018.03.008.

Santini, E., Feyder, M., Gangarossa, G., Bateup, H.S., Greengard, P., and Fisone, G. (2012). Dopamine- and cAMP-regulated phosphoprotein of 32-kDa (DARPP-32)-dependent activation of extracellular signal-regulated kinase (ERK) and mammalian target of rapamycin complex 1 (mTORC1) signaling in experimental parkinsonism. J. Biol. Chem. *287*, 27806–27812. https://doi.org/10.1074/jbc.M112.388413.

Santini, E., Valjent, E., Usiello, A., Carta, M., Borgkvist, A., Girault, J.-A., Hervé, D., Greengard, P., and Fisone, G. (2007). Critical involvement of cAMP/DARPP-32 and extracellular signal-regulated protein kinase signaling in L-DOPA-induced dyskinesia. J. Neurosci. *27*, 6995–7005. https://doi.org/10.1523/JNEUROSCI.0852-07.2007.

Schroll, H., Vitay, J., and Hamker, F.H. (2014). Dysfunctional and compensatory synaptic plasticity in Parkinson's disease. Eur. J. Neurosci. *39*, 688–702. https://doi.org/10.1111/ejn.12434.

Schwindinger, W.F., Mihalcik, L.J.M., Giger, K.E., Betz, K.S., Stauffer, A.M., Linden, J., Herve, D., and Robishaw, J.D. (2010). Adenosine A2A receptor signaling and golf assembly show a specific requirement for the gamma7 subtype in the striatum. J. Biol. Chem. *285*, 29787–29796. https://doi.org/10.1074/jbc.M110.142620.

Sebastianutto, I., Maslava, N., Hopkins, C.R., and Cenci, M.A. (2016). Validation of an improved scale for rating L-DOPA-induced dyskinesia in the mouse and effects of specific dopamine receptor antagonists. Neurobiol. Dis. *96*, 156–170. https://doi.org/10.1016/j.nbd.2016.09.001.

Shen, W., Flajolet, M., Greengard, P., and Surmeier, D.J. (2008). Dichotomous dopaminergic control of striatal synaptic plasticity. Science *321*, 848–851. https://doi.org/10.1126/science.1160575.

Shen, W., Plotkin, J.L., Francardo, V., Ko, W.K.D., Xie, Z., Li, Q., Fieblinger, T., Wess, J., Neubig, R.R., Lindsley, C.W., et al. (2015). M4 muscarinic receptor signaling ameliorates striatal plasticity deficits in models of L-DOPA-induced dyskinesia. Neuron *90*, 1139–1773. https://doi.org/10.1016/j.neuron.2016.05.017.

Siokas, V., Aloizou, A.M., Tsouris, Z., Liampas, I., Liakos, P., Calina, D., Docea, A.O., Tsatsakis, A., Bogdanos, D.P., Hadjigeorgiou, G.M., and Dardiotis, E. (2021). ADORA2A rs5760423 and CYP1A2 rs762551Polymorphisms as risk factors for Parkinson's disease. J. Clin. Med. *10*, 381. https://doi.org/10.3390/jcm10030381.

Solís, O., Garcia-Montes, J.R., González-Granillo, A., Xu, M., and Moratalla, R. (2017). Dopamine D3 receptor modulates l-DOPA-induced dyskinesia by targeting D1 receptor-mediated striatal signaling. Cereb. Cortex *27*, 435–446. https://doi.org/10.1093/cercor/bhv231.

Tanimura, A., Pancani, T., Lim, S.A.O., Tubert, C., Melendez, A.E., Shen, W., and Surmeier, D.J. (2018). Striatal cholinergic interneurons and Parkinson's disease. Eur. J. Neurosci. *47*, 1148–1158. https://doi.org/10.1111/ejn.13638.

Taverna, S., Ilijic, E., and Surmeier, D.J. (2008). Recurrent collateral connections of striatal medium spiny neurons are disrupted in models of Parkinson's disease. J. Neurosci. *28*, 5504–5512. https://doi.org/10.1523/JNEUROSCI.5493-07.2008.

Thiele, S.L., Chen, B., Lo, C., Gertler, T.S., Warre, R., Surmeier, J.D., Brotchie, J.M., and Nash, J.E. (2014). Selective loss of bi-directional synaptic plasticity in the direct and indirect striatal output pathways accompanies generation of parkinsonism and l-DOPA induced dyskinesia in mouse models. Neurobiol. Dis. *71*, 334–344. https://doi.org/10.1016/j.nbd.2014.08.006.

Tozzi, A., Tantucci, M., Marchi, S., Mazzocchetti, P., Morari, M., Pinton, P., Mancini, A., and Calabresi, P. (2018). Dopamine D2 receptor-mediated neuroprotection in a G2019S Lrrk2 genetic model of Parkinson's disease. Cell Death Dis. *9*, 204. https://doi.org/10.1038/s41419-017-0221-2.

Valjent, E., Corvol, J.C., Pages, C., Besson, M.J., Maldonado, R., and Caboche, J. (2000). Involvement of the extracellular signal-regulated kinase cascade for cocaine-rewarding properties. J. Neurosci. *20*, 8701–8709. https://doi.org/10.1523/JNEUROSCI.20-23-08701.2000.

Wang, Y., and Zhou, F.M. (2017). Striatal but not extrastriatal dopamine receptors are critical to dopaminergic motor stimulation. Front. Pharmacol. *8*, 935. https://doi.org/10.3389/fphar.2017.00935.

Wang, Z., Kai, L., Day, M., Ronesi, J., Yin, H.H., Ding, J., Tkatch, T., Lovinger, D.M., and Surmeier, D.J. (2006). Dopaminergic control of corticostriatal long-term synaptic depression in medium spiny neurons is mediated by cholinergic interneurons. Neuron *50*, 443–452. https://doi.org/10.1016/j.neuron.2006.04.010.

Wennogle, L.P., Hoxie, H., Peng, Y., and Hendrick, J.P. (2017). Phosphodiesterase 1: a unique drug target for degenerative diseases and Cognitive dysfunction. Adv. Neurobiol. *17*, 349–384. https://doi.org/10.1007/978-3-319-58811-7_13.

Westin, J.E., Vercammen, L., Strome, E.M., Konradi, C., and Cenci, M.A. (2007). Spatiotemporal pattern of striatal ERK1/2 phosphorylation in a rat model of L-DOPA-induced dyskinesia and the role of dopamine D1 receptors. Biol. Psychiatry *62*, 800–810. https://doi.org/10.1016/j.biopsych.2006.11.032.

Won, L., Ding, Y., Singh, P., and Kang, U.J. (2014). Striatal cholinergic cell ablation attenuates L-DOPA induced dyskinesia in parkinsonian mice. J. Neurosci. *34*, 3090–3094. https://doi.org/10.1523/JNEUROSCI.2888-13.2014.

Xu, M., Moratalla, R., Gold, L.H., Hiroi, N., Koob, G.F., Graybiel, A.M., and Tonegawa, S. (1994). Dopamine D1 receptor mutant mice are deficient in striatal expression of dynorphin and in dopamine-mediated behavioral responses. Cell *79*, 729–742. https://doi.org/10.1016/0092-8674(94)90557-6.

STAR★METHODS

KEY RESOURCES TABLE

REAGENT OR RESOURCE	SOURCE	IDENTIFIER
Antibodies		
mouse anti-tyrosine hydroxylase	Santa Cruz Biothechnology	Cat# sc-25269; RRID:AB_628422
rabbit anti-p-rpS6$^{S235/236}$	Cell Signaling	Cat# 2211S; RRID:AB_331679
rabbit anti-p-rpS6$^{S240/244}$	Cell Signaling	Cat# 2215S; RRID:AB_331682
mouse anti-c-*fos*	Abcam	Cat# ab190289; RRID:AB_2737414
mouse anti-p-44/42 MAPK (pERK$^{42/44}$)	Cell Signaling	Cat# 9101; RRID:AB_331646
goat anti-choline acetyltransferase	Millipore/Sigma	Cat# AB144P; RRID:AB_2079751
Cy3-coupled donkey anti-goat	Abcam	Cat# ab6949, RRID:AB_955018
Alexa 488-coupled goat anti-rabbit	Invitrogen	Cat# A-11034; RRID:AB_2576217
Alexa 488-coupled goat anti-mouse antibody	Invitrogen	Cat# A-11001, RRID:AB_2534069
Alexa 546-coupled goat anti-mouse	Invitrogen	Cat# A-11003; RRID:AB_141370
Alpha Tubulin Monoclonal antibody anti mouse	Protein Tech	Cat# 66031-1-Ig RRID:AB_11042766
Rabbit anti-Lrrk2 MJFF2(c41-2)	Abcam	Cat# Ab133474 RRID:AB_2713963
Chemicals, peptides, and recombinant proteins		
Tween 80	Sigma-aldrich	Cat# P1754-25ML
L-Dopa: L-3,4-Dihydroxyphenylalanine methyl ester hydrochloride	Sigma-aldrich	Cat# D1507
Benserazide-HCl	Sigma-aldrich	CAT# B7283-1G
VU 0255035-HCl		
VU 0467154	Med Chem Express	CAT# HY-112209
6-OHDA: 6-Hydroxydopamine hydrochloride	Sigma-aldrich	CAT# H4381
Nutra-Gel Diet	Bioserv	CAT# S4798-TRAY
Trizol- Reagent	ThermoFisher	CAT#15596018
Isoflurane	Patterson Veterinary	CAT#07-893-8440
Deposited data		
RNA-SEQ data	This paper	E-MTAB-11848 https://www.ebi.ac.uk/arrayexpress/

RESOURCE AVAILABILITY

Lead contact

For further information and requests for resources and reagents should be directed to and will be fulfilled by the lead contact, Prof. Emiliana Borrelli (borrelli@hs.uci.edu).

Materials availability

All unique/stable materials and models generated from this study are available from the lead contact with a completed Materials Transfer Agreement.

Data and code availability

- All data reported in this paper will be shared by the lead contact upon request.

- The RNA-SEQ data are available at https://www.ebi.ac.uk/arrayexpress/ with the accession number: E-MTAB-11848.
- This paper does not report original code. The URL of the codes used in this paper are listed in the key resources table.
- Any additional information required to reanalyze the data reported in this paper is available from the lead contact upon request.

EXPERIMENTAL MODEL AND SUBJECT DETAILS

Mutant iMSN-D2RKO mice were generated by mating $D2R^{flox/flox}$ males with $D2R^{flox/flox}$ females carrying the CRE under the control of the D1 receptor promoter (D1)-Cre. This way, we generated the $D2R^{flox/flox}/^{D1-Cre/+}$ line; the $D2R^{flox/flox}$ mice are thereafter called WT in our study (Anzalone et al., 2012). The D1R gene is expressed during development in MSNs precursors (Aizman et al., 2000) allowing the deletion of D2R as previously shown selectively in iMSNs (Anzalone et al., 2012). Mutant and control mice used in this study were in the same genetic background (98.4% C57BL6 X 1.56% 129 SV). Eight-to fifteen-weeks-old male iMSN-D2RKO and WT mice, weighting between 25-30 g at the beginning of the study, were used. Mice were group housed and maintained at standard 12h/12h light/dark cycle, at ~25°C, and humidity levels at 45%–60%, with standard food and water *ad libitum*. Females iMSN-D2RKO and WT did not differ in the expression of L-DOPA-induced AIMs, as compared to male mice, thereafter all experiments were performed in males. All protocols were submitted and approved by the University of California, Irvine Institutional Animal Care and Use Committee in accordance with the National Institute of Health and the ARRIVE guidelines.

METHOD DETAILS

Chemical and reagents

L-DOPA (Sigma), benserazide-HCl (Sigma), and VU 0255035-HCl (UCI) were dissolved in physiological sterile saline (0.9% NaCl), VU 0467154 (MedChemExpress) was dissolved in Tween 80 (Sigma) 10% w/v and physiological sterile saline (0.9% NaCl). Compounds were injected either subcutaneously (s.c., for L-DOPA and benserazide) or intraperitoneally (i.p., for VU 0255035-HCl and VU 0467154), using a volume of 10 mL/kg of body weight. Controls received an equivalent volume of saline. 6-OHDA (Sigma) was dissolved in sterile saline containing 0.05% of ascorbic acid to reduce molecule oxidation. For electrophysiological evaluations, VU 0255035-HCl (UCI) was dissolved in dimethlysulfoxide (DMSO) to 0.01%.

Unilateral 6-OHDA stereotaxic surgery

WT and iMSN-D2RKO mice (25–30g) were anesthetized with a mixed of vaporized isoflurane/air 3% (Kent Scientific) before being placed in a stereotaxic frame equipped with a mouse adaptor (model 963, David Kopf Instruments). Afterward, a nose cone was placed over the mouse and isoflurane/air concentration was lowered to 1%–2%. Temperature and breathing were closely monitored throughout the surgery.

Each mouse received either two unilateral injections (inj.) of 2μL of 6-OHDA into the right DLS (coordinates in mm relative to bregma: 1^{st} inj. anteroposterior (AP): +1.0, mediolateral (ML): -2.1, dorsoventral (DV): -2.9 and 2^{nd} inj. AP: +0.3, ML: −2.3, DV: −2.9) or one unilateral inj. of 1μL of 6-OHDA into the right MFB (AP: −1.2, ML: −1.2, DV: −4.75) according to the Paxinos and Franklin (2001) mouse brain atlas (Francardo et al., 2011). 6-OHDA was dissolved in ice-cold sterile saline containing 0.05% of ascorbic acid to obtain a concentration of 3 mg/mL (calculated as free base). 6-OHDA was delivered by a 10 μL WPI syringe (equipped with a 35G needle) connected to an external pump (UMC4, WPI; flow rate: 250 μL/min). After each 6-OHDA injection, needle was left in place for 10 min to optimize tissue retention. Following surgery, mice received for two weeks daily post-operative care consisting of two injections of sterile dextrose-saline solution (2.5g/50mL, s.c., 6–8 h spaced) and the addition of a highly palatable gel food (Nutra-Gel Diet, s4798). Mice that showed difficulties in eating due to severe postural asymmetry were hand-fed.

Behavioral analyses

Open field test

To obtain a preliminary estimation of 6-OHDA-induced dopaminergic degeneration, two weeks after surgeries, WT and iMSN-D2RKO mice were individually placed for 10 min in a white wooden box (30X30X30 cm; 70 lux) to track and record their horizontal locomotor activity by the mean of a

video-tracking automated system (Viewpoint Behavior Technology; Lyon France). In addition, footages were further analyzed to count the total number of ipsilateral and contralateral turns to the lesion (used as index of asymmetry) performed by each mouse over ten minutes. 180-degree turns were scored as one, while 360-degree turns were score as two (Francardo et al., 2011). Behavioral analyses were performed by an expert observer blind to the mouse genotype.

Abnormal involuntary movements evaluation

AIMs evaluation was based on a well-established rating scale specifically designed to test L-DOPA induced dyskinesia severity in hemi-parkinsonian rodents (Francardo et al., 2011). Behavioral analyses were performed by an expert observer blind to the mouse genotype.

Mice were individually placed in transparent cages (20 cm x 30 cm x 12 cm) without bedding material and observed for 1 min every 20 min over a total period of 120 min, immediately after L-DOPA administration. AIMs clearly different from natural stereotyped movements were classified into four subtypes according to their topographic distribution: axial (dystonic posturing of the upper part of the body toward the side contralateral to the lesion), limb (abnormal movement of the forelimb contralateral to the lesion), and orolingual AIMs (vacuous jaw movements and tongue protrusions toward the side contralateral to the lesion). Each subtype was scored based on a frequency-based scale ranging from 0 to 4, defined as follows: 0, absent; 1, present less than half of the observational period; 2, present more than half of the observational period; 3, continuous but interruptible by external stimuli; 4, continuous and not interruptible by external stimuli, for a maximum score of 12 for each minute of observation. The total AIMs score for each session was obtained by summing individual partial scores.

Experimental Plan

Experiments were carried out in unilateral 6-OHDA WT and iMSN-D2RKO mice, and sham controls, to assess: (1) the involvement of D2Rs in iMSNs in the development and expression of AIMs following L-DOPA; (2) the influence derived by the surgical procedure (striatal vs MFB 6-OHDA infusion) and L-DOPA dosage (low dose vs high dose) on AIMs expression; (3) the contribution of the cholinergic system in LID.

Experiments (1) were performed in WT and iMSN-D2RKO littermates unilaterally subjected either to sham or 6-OHDA lesions in the right DLS. Three weeks after surgeries, mice received a daily injection of L-DOPA (15 mg/kg; s.c.) plus benserazide (12 mg/kg; s.c.) for 11 consecutive days. AIMs were assessed on day one, four, seven and ten of L-DOPA treatment. The eleventh day, mice were sacrificed either after 30 min from L-DOPA for subsequent immunohistochemical analyses, or after 60 min from L-DOPA for Western blot and RNAseq analyses. Additionally, a subgroup of control, sham and 6-OHDA WT and iMSN-D2RKO mice were used for electrophysiological evaluations.

Experiments (2) were performed in WT and iMSN-D2RKO mice unilaterally subjected either to sham or 6-OHDA lesion in the right MFB. Three weeks after surgeries, mice received escalating doses of L-DOPA (1.5, 3, and 6 mg/kg, s.c., dose was changed every three days) plus benserazide (12 mg/kg; s.c.) over nine consecutive days. AIMs evaluation was performed after each L-DOPA administration.

For experiments (3), we tested: (A) the acute anti-dyskinetic effects produced by a high dose of the selective M1R antagonist VU 0255035 in already dyskinetic WT and iMSN-D2RKO mice. 6-OHDA WT and iMSN-D2RKO mice were rendered dyskinetic by treating them for five consecutive days with L-DOPA (15 mg/kg, s.c.) plus benserazide (12 mg/kg, s.c.); then, mice received 10 days of drug wash-out in their home cage. Afterward, mice received in acute VU0255035 (15 mg/kg, i.p.) or its vehicle (saline) 15 min before the L-DOPA (6 mg/kg, s.c.) plus benserazide (12 mg/kg, s.c.). (B) the sub-chronic anti-dyskinetic effects produced by the combined administration of the M1R antagonist VU 0255035 and the M4R PAM VU0467154 in already dyskinetic WT and iMSN-D2RKO mice. 6-OHDA WT and iMSN-D2RKO mice were rendered dyskinetic as previously described in (A). After 10 days of drug wash-out in their home cage, mice received six daily injections of VU0467154 (10 mg/kg; i.p.), either alone or in association with VU0255035 (15 mg/kg; i.p.), 15 min before L-DOPA (6 mg/kg; s.c.) plus benserazide (12 mg/kg; s.c.). AIMs were assessed on day one, three, and six of treatment.

Immunofluorescence

Thirty minutes after the last L-DOPA administration, mice were deeply anaesthetized with Euthasol (Virbac AH, Inc., Fort Worth, TX) and transcardially perfused with cold 4% paraformaldehyde dissolved in sterile phosphate-buffered saline (PBS, Na2HPO4 10 mM, KH2PO4 1.8 mM, NaCl 137 mM, KCl 2.7 mM). Whole brains were then post-fixed over-night in 4% paraformaldehyde in PBS at 4°C. 30μm coronal brain sections were made using a vibratome (Leica) and stored in cryoprotectant solution (30% glycerol and 30% ethylene glycol in PBS) at −20°C until use. For each mouse, three representative sections were collected from the striatum (1.34 to 0.74mm from Bregma) and the SNc (−2.92 to −3.52mm from Bregma), according to the Paxinos and Franklin (2001) mouse brain atlas.

Free floating sections were first washed three times (8 min each) in tris-buffered saline (TBS; 0.25 M tris and 0.5 M NaCL, pH 7.5), blocked in a solution containing 5% normal goat serum, 0.05% bovine serum albumin, and 0.3% Triton X-100 at room temperature for one hour. Afterward, sections were incubated with the primary antibodies: mouse anti-tyrosine hydroxylase (TH) (1:1000, Santa Cruz Biothechnology), rabbit anti-p-rpS6-S240/244 (1:600, Cell Signaling), mouse anti-c-Fos (1:1000, Abcam), mouse anti-p-44/42 MAPK (1:200, Cell Signaling), goat anti-choline acetyltransferase (1:500, Millipore) in TBS 1% NGS overnight at 4°C, either alone or in combination. The following day, sections were first rinsed three times in TBS for 10 min and then incubated for 1 h at RT with the appropriate secondary antibody: Cy3-coupled donkey anti-goat (1:800, Abcam), Alexa 488-coupled goat anti-rabbit (1:800, Invitrogen), Alexa 488-coupled goat anti-mouse antibody (1:800, Invitrogen), Alexa 546-coupled goat anti-mouse (1:800, Invitrogen) in TBS 1% NGS. Sections were rinsed twice with TBS before nuclei were stained with Draq 7 (1:1000; Biostatus), and glass-mounted using the Prolong Gold solution (Thermofisher). Images from the DLS were taken on an SP5 confocal microscope (Leica), while images from the SNc were taken from a fluorescent microscope (Leica). Neuronal quantification and measurement of the mean intensity x cell for neurons positive for c-Fos, pERK42/44, and p-rpS6-S240/244 were performed in three 387.5 × 387.5 μm images covering the entire DLS (three striatal sections/mouse were used). Neuronal quantification of TH + neurons was performed in two 1,243.8 × 932.73 μm images covering the entire SNc (three striatal sections/mouse were used). Quantification of immunoreactive neurons was carried out by the manual particle counting option of Image J software (U.S. National Institutes of Health, USA), in experimenter blinded analyses. Measurement of the intensity x cell of immunoreactive neurons was carried out by manually drawing a region of interest around the perimeter of each individual neuron by the freehand selection tool of ImageJ software. Afterward, the mean intensity value x cell was obtained, and background subtracted.

Western blot

Frozen tissue punches of the striatal region were homogenized and sonicate for 3 rounds at 60% of intensity in Radioimmunoprecipitation assay buffer (RIPA buffer) + protease inhibitor. The proteins were quantified using Varioskan™ LUX multimode microplate reader. 10 μg of proteins were separated on SDS-PAGE 6% and transferred onto membranes. Primary antibodies used were: Rabbit anti-Lrrk2 MJFF2(c41-2) abcam (Cat# Ab133474) (1:5000) and mouse anti-aTubulin (ProteinTech Cat# Cat# 66031-1-Ig) (1:20000). Secondary HRP anti-rabbit and/or anti-mouse antibodies (1:5000) were from Millipore (Millipore, Cat# AQ132P). Western blots were revealed using ChemiDoc Imagers (Biorad, USA), and the quantifications were performed using the "Image Lab" software (Biorad, USA).

RNA preparation for RNA-sequencing

For RNA-seq, the last day of the experiments and 1h after L-DOPA injections, brains were dissected and rapidly frozen in 2-methylbutane on dry ice. Unilateral tissue punches from the DLS of the right hemispheres of mice treated in the different conditions tested were obtained and rapidly homogenized in Trizol (Thermo Fisher) using a 26 1⁄2 gauge needle attached to a 1 mL syringe. RNA isolation was completed following the Trizol (Thermo Fisher) manufacturer's protocol. RNA was resuspended in H_2O.

Library preparation for RNA-Sequencing

Library preparation and sequencing were performed at the University of California, Irvine Genomic High-Throughput Facility. Total RNA was monitored for quality control using the Nanodrop absorbance ratios for 260/280nm and 260/230nm and the RIN (RNA Integrity Number) was evaluated with Agilent Bioanalyzer Nano RNA chip. Library construction was performed according to the Illumina TruSeq Stranded mRNA Sample Preparation Guide. The input quantity for total RNA was 150 ng and mRNA was enriched using

oligo dT magnetic beads. The enriched mRNA was chemically fragmented for three minutes. The first strand synthesis used random primers and reverse transcriptase to make cDNA. After second-strand synthesis, the double-stranded cDNA was cleaned using AMPure XP beads and the cDNA was end-repaired and then the 3-ends were adenylated. Illumina barcoded adapters were ligated on the ends and the adaptor-ligated fragments were enriched by nine cycles of PCR. The resulting libraries were validated by qPCR and sized by Agilent Bioanalyzer DNA high sensitivity chip. The concentrations for the libraries were normalized and then multiplexed together. The multiplexed libraries were sequenced on four lanes using single end 100 cycles chemistry on the HiSeq 4000. The version of HiSeq control software was HCS 3.4.0.38 with real-time analysis software.

Bioinformatics

Read quality was assessed by FastQC software. Sequence alignment was performed using the *Mus musculus* GENCODE reference genome (GTF file from release M23 GRCm38.p6) using STAR 2.6.0c software. Differential expression analysis was performed using the DESeq2 tool for "R". Read counts were normalized using the relative log expression method of DESeq2. All software and tools were used with default parameters. Normalized read counts were converted into the log-read counts, which were then used for identifying differentially expressed genes; in all our comparisons a Log2 Fold-Change +/− 20% with an adjusted p value < 0.1 was considered statistically significant. KEGG pathway analyses were performed using "Enrichr" tool (https://maayanlab.cloud/Enrichr/), (Chen et al., 2013) with a significance p value < 0.05.

Field Potential Recordings

Striatal slices were prepared from male iMSN-D2RKO and WT mice (approximately 2 months of age). Following isoflurane anaesthesia, mice were decapitated, and the brain was quickly removed and submerged in ice-cold, oxygenated dissection medium containing (in mM): 124 NaCl, 3 KCl, 1.25 KH_2PO_4, 5 $MgSO_4$, 0 $CaCl_2$, 26 $NaHCO_3$, and 10 glucose. Coronal slices (340 μm) were prepared using a Leica vibrating tissue slicer (Model: VT1000S) before being transferred to an interface recording containing pre-heated artificial cerebrospinal fluid (aCSF) of the following composition (in mM): 124 NaCl, 3 KCl, 1.25 KH_2PO_4, 1.5 $MgSO_4$, 2.5 $CaCl_2$, 26 $NaHCO_3$, and 10 glucose and maintained at 31 ± 1^0C. Slices were continuously perfused with this solution at a rate of 1.75–2 mL/min while the surface of the slices were exposed to warm, humidified 95% O_2/5% CO_2. Recordings began following at least 2 h of incubation.

Field potential recordings were conducted in control (no surgery), sham- and 6-OHDA-lesioned iMSN-D2RKO and WT mice containing the DLS. Extracellular recordings were measured in the presence of the GABA-A receptor antagonist picrotoxin (50 mM), with micropipettes (2.0 MΩ) filled with 1 M NaCl. A twisted bipolar electrode was placed in the DLS near the border of the external capsule. Following a 10 min stable baseline recording, LTD was induced by delivering a single train of low-frequency stimulation (LFS; 10 Hz for 10 min). The magnitude of LTD was calculated by comparing the average 10 min baseline responses with the average responses recorded 30–40 min post-LTD induction. Data were collected and digitized by NAC 2.0 Neurodata Acquisition System (Theta Burst Corp., Irvine, CA) and stored on a disk.

QUANTIFICATION AND STATISTICAL ANALYSIS

All values are presented as mean ± SEM. GraphPad Prism 9 (La Jolla California, USA) was used to perform statistical analyses. For each analysis, normality of residues and homoscedasticity were assessed. Depending on the Gaussian distribution of our data, we employed either the parametric two-tailed t-test or the non-parametric Mann-Whitney U test for comparison between two groups. To examine the influence of two independent variables (e.g. time X genotype) on our results, we employed the Two-way Analysis of Variance (ANOVA), or Two-way repeated measures (RM) ANOVA followed by Bonferroni's, or Newman-Keuls's multiple comparison post hoc test. For RM tests, whenever we could not assume sphericity, a Geisser–Greenhouse correction was carried out. $p < 0.05$ was considered statistically significant.